**MINISTRY OF HIGHER EDUCATION AND SCIENTIFIC RESEARCH**

**LARBI BEN M'HIDI UNIVERSITY, OUM EL BOUAGHI**

**FACULTY OF EXACT SCIENCES NATURAL SCIENCES AND LIFE**

**DEPARTMENT OF SCIENCES OF MATTER**

**Ordre N° : M……. /2023**

# Dissertation

Presented to obtain

The Degree of Academic Master

Option: **physics of materials**

**THEME**

# Preparation by sol-gel process of ZnO/$TiO_2$Nanocomposite and its activity for Methyl Orange Degradation

Realized by:

**Djeddi Nassira** **Telili Zahra**

Under the direction of: **Moualkia Hassiba**

Defended on: 25/06/2023

Jury committee:

| | | |
|---|---|---|
| Prof Azizi Cherifa | Oum El Bouaghi University | President |
| Prof Moualkia Hassiba | Oum El Bouaghi University | Supervisor |
| Prof Mecif Abla | Oum El Bouaghi University | Examiner |

**College Year: 2022/2023**

# *Acknowledgements*

*This thesis was carried out within the laboratory of materials and structure of electromechanical systems and their reliability, of the department of material sciences, Unversity Larbi Ben M'hidi Oum El Bouaghi.*

*First of all, we would like to thank ALLAH, the only one who gave us the patience, the will and the courage to carry out this research work.*

*Our deep gratitude goes particulary to our supervisor Prof* ***MOUALKIA HASSIBA****, professor of phisics at the University Larbi Ben M'hidi Oum El Bouaghi for her guidance and invaluable help.*

*We would like to sincerely thank Prof* ***AZIZI CHERIFA*** *Professor at Larbi Ben M'hidi Oum El Bouaghi University, for agreeing to chair the jury of defense and to judge this work. Our thanks are also addressed to* ***MECIF ABLA*** *Professor at Larbi Ben M'hidi University for agreeing to be part of the jury and evaluate our work.*

*We would like to sincerely thank Dr* ***MECHEHOUD NAIMA****, professor of chemistry at Al-Hadj Lakhdar Unversity, Batna-1-, and Dr* ***BENZITOUNI SARA*** *for their assistance in the implementation and completion of this work.*

*We would like to express our gratitude to the following people, for their help in completing this dissertation :*

*Prof* ***L. REMACHE*** *director of the laboratory (LMSES) University of Oum El Bouaghi.*

*Ms* ***KARIMA*** *and* ***MABROUKA****, engineers from the chemistry-physics Laboratory, Hadj Lakhdar University, Batna-1-.*

*Finally, Our thanks also go to all the teachers in the physics field for the training they provide to us throughout our course university.*

# *Dedication*

*I dedicate this thesis to:*

*To the dearest being of my life « **My MotherYASMINA** » who has always supported me by his love, and who was always by my side in difficult times*

*-رحمها الله -*

*To who always supported me since the beginning of my studies, may Allah keep you a blessing in my life to my great **DAD**.*

*To my dear sisters **MALIKA**, **FATIMA ZOHRA** and **WIDAD** for their encouragement and their moral support.*

*To my dear brothers, **SALAH EL DINNE**, **BILAL** and **IYAD** who have always been the source of inspiration and encouragement.*

*To my little angel of **ALLA RAHMAN**, your presence has given me strength and courage. You are my motivation in life.*

*To my best friend, who has always been by my side in good and bad times to my partner **ZAHRA.***

*To all my professors, especially the professor **A.MAHDJOUB**.*

Nassira

# *Dedication*

*I dedicate this thesis to:*

*To the most precious two in my life, who gave me everything, who built me up to who I am today, to the one who has always supported me since the beginning of my studies, My God keep you as a blessing in my life to my wonderful* ***MOM*** *Andmy great* ***DAD****.*

*To my dear sisters* ***FAIZA, SAMRA****, and* ***SAMIRA*** *for their encouragement and their moral support.*

*To my dear brothers,* ***RIAD****,* ***YACINE*** *and* ***FATEH*** *who have always been the t source of inspiration and encouragement.*

*To honorable professor* ***A. MAHDJOUB.***

*To all my BTS , SJ, SNSD ,friends , 0those who have always been by my side in good and bad times ,who always lifted my mood and who made me a happy bright girl*

*To my partner* ***NASSIRA.***

*To all my teachers who taught me along my studies*

Zahra

# Table of Contents

## Liste of tables

**Liste of figures**

| **Chapter III** | | |
|---|---|---|
| **Figure III.1** | $X$RD spectra of (ZnO/$TiO_2$) nanocomposites prepared with different percentages of (ZnO and $TiO_2$). | **57** |
| **Figure III.2** | Single cubic lattice. | **58** |
| **Figure III.3** | Gaussian adjustment method of diffraction peaks, ($Xc$ = 2θ ; = $Int$and$W$ = $FWHM$). | **59** |

# General Introduction

# General Introduction

In recent years, the most common problem that human beings are frequently facing is the scarcity of clean water which is thought to be caused due to climate change and poor water resource management. So, a mandatory issue has been arisen to implement the reclamation of these unclean water. Initially, various water treatment techniques for example: adsorption, reverse osmosis, membrane separation…etc. But these techniques failed to provide sufficient satisfaction due to their costing issues and also their incapability to annihilate the wastes from the water, especially the organic pollutants. Nowadays, several cost-effective advanced oxidation processes such as: fenton /photo-fenton oxidation, ozonation, and photocatalysis

Among these processes, the photocatalysis is often considered to be the most effective way for the disinfection of wastewater. Generally it utilizes oxide semiconductors for example: $Fe_2O_3$, ZnO, $TiO_2$, $CeO_2$, $WO_3$..….. etc [1].

Zinc oxide (ZnO) and titanium dioxide ($TiO_2$) are n-type semiconductor oxides that have attracted a lot of research interest. Both ZnO and $TiO_2$ possess outstanding physical and chemical properties such as non-toxicity and high reactivity at the nanoscale. Furthermore, both are highly earth-abundant, and hence cheap. ZnO and $TiO_2$ also exhibit wide bandgaps of 3.37 and 3.2 ev (anatase), respectively [2,3,4].A good number of researches have been carried out to eliminate pollutants making use of both ZnO and $TiO_2$ catalysts. Higher photocatalytic efficiency of ZnO compared with $TiO_2$ has been reported [5].

$TiO_2$ in the anatase phase shows excellent photocatalytic activity and is widely used for photocatalytic processes like water-treatment and air-purification. This is because it has a high oxidizing potential for the photo degradation of organic and inorganic compounds and dyes. ZnO also exhibits high photocatalytic activity and can effectively decompose certain compounds even in the dark.

Unfortunately, the photocatalytic efficiencies of both $TiO_2$ and ZnO are limited by certain factors. Their wide bandgaps permit UV light absorption only at wavelengths lower than or equal to 385 nm ($\lambda \leq 385$ nm). In addition, the high recombination rate of the electron-hole pairs generated by these oxides also degrades their photocatalytic efficiency [4,6].

To overcome this limitation, various efforts have been made to develop nanocomposites containing both these oxides. Such nanocomposites can absorb visible light with wavelengths ≥ 400 nm and also offer enhanced charge separation [6].

Coupled semiconductor photocatalysts is a novel approach to achieve a more efficient charge separation, an increased lifetime of the charge carriers, and an enhanced interfacial charge transfer to adsorbed substrates [7].At the same time, their physical and optical properties are greatly modified [8].It is expected that the nanocomposites composed of ZnO and $TiO_2$ nanoparticles exhibit useful applications in photocatalysis and an improvement in the photocatalytic activity.

In this study, we synthesized a ZnO/$TiO_2$nanocomposites with excellent photocatalytic properties via a reproducible, cost-effective, and versatile modified sol-gel technique.
We prepared two sets (series) of samples:

- ✓ In the first series we varied the composition of ZnO and $TiO_2$ to obtain the nanocomposites of ZnO/$TiO_2$. ZnO percentages are: 85, 80, 75 and 65%, $TiO_2$ percentages are: 15, 20, 25 and 35%. The different samples with the different percentages are: 85%ZnO/15%$TiO_2$, 80%ZnO/20%$TiO_2$, 75%ZnO/25%$TiO_2$, 65%ZnO/35%$TiO_2$, these samples are calcinated at a low temperature of 300°C, the calcination time is two hours.
- ✓ However, the second series presents the 80%ZnO/20%$TiO_2$ sample with different calcination temperatures (300, 700, 750, 800, 850 and 900°C), the calcination time is two hours.

As an application the prepared samples are used for the photocatalytic degradation of a dye methyl orange.

This manuscript has been divided into three chapters:

- ❖ The first chapters are devoted to presenting a bibliographic study giving a general overview around ZnO and $TiO_2$ and their physical properties, as well as a complete explanation of the sol-gel technique, finally, an overview of photocatalytic degradation and the used dye.

- The second chapter is devoted (i) we have described the progress of the stages of realization of the experiment with the photos (ii) to the exposure of the different characterization methods used to analyze our samples.
- The third chapter, we finish this manuscript with collecting and discussing all the results obtained along this study.

Finally, the dissertation ends with a general conclusion.

**References**

[1] M.A. Mintu, MD.J. Haque, M.H. Kabir, M.A. Kaiyum, M.S. Rahman, Nanosynthesis of ZnO-$TiO_2$ composites by sol-gel method and evaluation of their antibacterial, optical and photocatalytic activities, results of materials ,11, (2021), p100199.

[2] A. Kołodziejczak-Radzimska and T. Jesionowski, Zinc Oxide−from Synthesis to Application: A Review, Materials, 7(4), (2014), p 2833-2881.

[3] O. Oprea, E. Andronescu, D. Ficai, A. Ficai, F. N. Oktar, and M. Yetmez, "ZnO Applications and Challenges, Curr.Org. Chem., 18, (2014), p192-203.

[4] M. Pelaez, N.T. Nolan, S.C. Pillai, M.K. Seery, P. Falaras, A.G. Kontos, P.S.M. Dunlop, J. W. J. Hamilton, J. A. Byrne, K. O'Shea, M. H. Entezari, and D. D. Dionysiou, A Review on the Visible Light Active Titanium Dioxide Photocatalysts for Environmental Applications ,Appl. Catal., B, 125, (2012), p 331-349.

[5] S.K. Kansal, M. Singh, D. Sud, Studies on $TiO_2$/ZnO photocatalysed degradation of lignin , Journal of Hazardous Materials,153, (2008), p 412–417.

[6] M.A. Habib, M.T. Shahadat, N.M. Bahadur, I.M.I. Ismail, and A.J. Mahmood, Synthesis and Characterization of ZnO-$TiO_2$Nanocomposites and Their Application as Photocatalysts, International Nano Letters 3, 5, (2013).

[7] O. Carp, C.L. Huisman, A. Reller, Photoinduced reactivity of titanium dioxide, Progress in Solid State Chemistry, 32, (2004), p 33–177.

[8] X.Z. Li, F.B. Li, C.L. Yang, W.K. Ge, Photocatalytic activity of $WO_x$-$TiO_2$ under visible light irradiation ,Journal of Photochemistry and Photobiology A: Chemistry ,141, (2001), p 209–217.

# Chapter I

# Bibliographic study

## I.1.Introduction

In this chapter, present a bibliographic study of zinc oxide (ZnO) and titanium dioxide ($TiO_2$) and their various applications. First, we give an overview of nanocomposites. Next, we detail the properties, and the main fields of application of zinc oxide and titanium dioxide, after that we present a quick background on the method of synthesis « Sol-Gel ». Finally, we provide an overview of photocatalytic.

## I.2.Nanomaterials and Nanocomposites

### I.2.1.Nanomaterials

#### I.2.1.1. Definition

In recent decades, « nano » become a more and more widely used word in our life. It comes from the Greek word vavos, in the Latin alphabet «nanos», which means dwarf and now it is used to describe objectives with the order of magnitude $10^{-9}$, unites.

Nanomaterials are materials in which at least one dimension, such as atomic density, grain size, chemical composition, scale or crystallographic orientation varies over a nanometric between 1 and 100 nm. Because of the promising applications in scientific research and industry area, lots of efforts have been applied in synthesize, control and functionalization works to obtain nanomaterials with outstanding properties which will make them do great contribution our social welfare [1].

#### I.2.1.2. Classification of Nanomaterials

Nanomaterials could be classified according to their morphology as shown in **Figure I.1**.

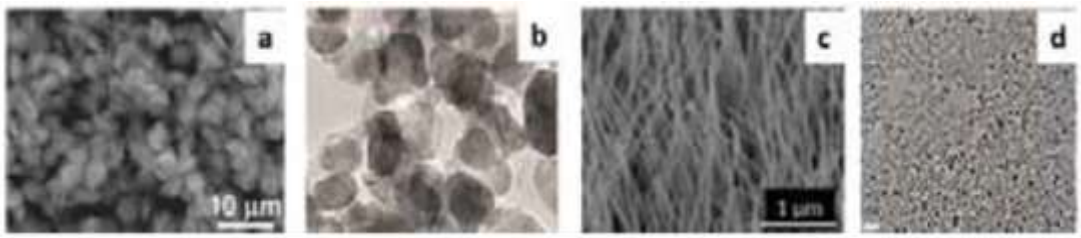


**Figure I.1.** SEM and TEM images of nanomaterials in different dimension (a) 3D, (b) 2D,(c)1D,(d)0D [1].

- 3D nanomaterials have all three dimensions in nano range. 3D nanomaterials include nanogranules, nanoclays and equiaxed nanoparticles.
- 2D nanomaterials have two dimensions in nano range. It is include nanofibers, nanotubes, nanorods and whiskers. Carbon nanotubes are good example of 2Dnanomaterials.
- 1D nanomaterials have at least one dimension in nano range. This leads to needle like –shaped materials having one dimension at nanoscale. It is include nanoplatelets, nanorods, nanoclays and nanosheets.
- 0D nanomaterials have all the dimension within nanoscale, i.e. no dimension is larger than 100 nm. The most common example of 0D-dimensional nanomaterials is the nanoparticle. These nanoparticles can be crystalline or amorphous, metallic, ceramic, or polymeric [2].

### I.2.2.Nanocomposites

#### I.2.2.1.History of nanocomposites

Nanocomposites have been studied for nearly 50 years, but few references address the importance of how the organoclay is processed into the plastic of choice. Nanocomposites were first as 1950, and polyamide nanocomposites were reported as early as 1976. Acquarulo& O'Neil (2002)[3] in their work observed that in the early 1980s that Toyota's Central Research and Development Laboratories began working with polymer - layered silicate - clay mineral composites and that the period was when the technology began to be studied more widely.

#### I.2.2.2. Definition

Nanocomposite is a multiphase solid material where one of the phases has one, two or three dimensions of less than 100 nanometers (nm) or structures having nano-scale repeat distances between the different phases that make up the material.

The idea behind Nanocomposite is to use building blocks with dimensions in nanometre range to design and create new materials with unprecedented flexibility and improvement in their physical properties.

In the broadest sense this definition can include porous media, colloids, gels and copolymers, but is more usually taken to mean the solid combination of a bulk matrix and nano-dimensional phase(s) differing in properties due to dissimilarities in

structure and chemistry. The mechanical, electrical, thermal, optical, electrochemical, catalytic properties of the nanocomposite will differ markedly from that of the component materials [4].

**I.2.2.3. Classification of Nanocomposites**

Nanocomposites can be classified into two categories: Non-polymer based nanocomposites and polymer based nanocomposites.

**a) Non-polymer based nanocomposites:** are also known as inorganic nanocomposites. And can be classified as follows :

- **Metal/Metal nanocomposites:** Bimetallic nanoparticles either in the form of alloy or core-shell structures or being investigated in some depth because of their improved catalytic properties and changes in the electronic/optical properties related to individual, separate metals. It is postulated their interesting Physico-chemical properties, result from the combination of two kinds of metals and their fine structures.
- **Ceramic/Ceramic Nanocomposites:** Ceramic Nano composites could solve the problem of fracture failures in artificial joint implants; these would extend patient's mobility and eliminate the high cost of surgery
- **Metal/Ceramic Nanocomposites:** In this type of composites, metal/ceramic nanocomposites have a chemically inert and hard ceramic matrix. Moreover, the electrical, magnetic, chemical, optical and mechanical properties of the two phases are combined

**b) Polymer based nanocomposites:** Polymer nanocomposites are composites with a polymer matrix and filler with at least one dimension less than 100 nm and can be classified as follows:

- **Polymer/ceramic nanocomposite:** Nanocomposites consist of single ceramic layers (1nm thick) homogeneously dispersed in a continuous matrix.
- **Metal/ polymer nanocomposites:** Metal polymer nanocomposites attract attention because of unique properties of metal clusters which are dispersed in polymer matrix. The typical size of such metal cluster is approximately $1^{-10}$ nm. The properties of clusters and nanoparticles (band gap, spectral properties, the transport of electrons) are very different from those of bulk materials and from individual atom or molecules.
- **Hybrid metal/polymernanocomposite:** Hybrid inorganic/organic materials are not simply physical mixtures, its nanocomposites with organic and inorganic components intimately mixed.

- **Layered silicate/ polymernanocomposites:** Polymer/Layered silicate (PLS) nanocomposites materials. In recent years the PLS nanocomposites have attracted great interest both in industry and academia, because they often exhibits remarkable improvements in materials when compare with virgin polymer and conventional macro and macro composites.
- **Polymer/polymer Nanocomposites:** Polymers are more than ever under pressure to be chip and offered property profiles. The gap between block co-polymer self assembly and offer nanostructured plastic endowed with still unexplored combinations of properties is getting narrower. Mixtures of different polymers often phase separate, even when their monomer mixed homogenously [5].

**I.2.2.4. Metal oxide based nanocomposites**

Generally utilizes oxide semiconductors that are inexpensive, non toxic and also have a wider band gap such as ZnO, $TiO_2$, $Fe_2O_3$, $SnO_2$, $SiO_2$….etc [6].

❖ **Mixed metal oxide nanocomposites**

When using semiconducting oxides separately, it was proven that they contain several defects, so it was modified with another metal oxide to improve its properties, which could lead to superior performance for various applications, including photocatalysis for example: ($TiO_2$/ZnO) where the resulting ZnO/$TiO_2$ nanocomposite showed better photocatalytic degradation of dye pollutants than pure ZnO and $TiO_2$ [7].

**I.2.2.5.Application of Nanocomposites**

The multiple properties and various advantages of nanocomposites led to interest, and use in several fields. We mention amongitis uses the following :

- Drug delivery systems.
- Anti-corrosionbarriercoatings.
- UV protection gels.
- Lubricants and scratch free paints.
- New fire retardant materials.
- New scratch/abrasion resistant materials.
- Superior strength fibres and films. [3]

## I.3. Zinc oxide (ZnO)

### I.3.1.General information on zinc oxide

Zinc oxide is a chemical compound with the formula ZnO made from 80.36% zinc and 9.66% oxygen. Its molar mass 81.38g/mol, its melting point 1975°C, its density 5.6 $g/cm^{-3}$ [8].

Zinc oxide (ZnO) is a non-toxic, non-toxic type (II-VI) binary material, wide direct gap (3.3eV) with high exciton binding energy (60meV). He istransparent in the visible and near infrared. It presents a set of properties that allow its use in a large number of applications. It can also find applications in optoelectronics, cathodoluminescence, and photoluminescence, electroluminescence, as a chemical probe in thin layers or as a piezoelectric material [9].

The material ZnO exists in a natural form, under the name "Zincite", but can also be artificially synthesized in massive form. Its color varies according to the impurities it contains and according to its deviation from stoichiometry as shown in **Figure I.2** [10].

**Figure I.2.** Zinc oxide (ZnO) in a) natural form, b) crystal structures, c) amorphous powder [10].

### I.3.2.The main advantages of ZnO

- High piezoelectric effect ($e^{33}$ = 1.2 $C/m^2$ among the highest of all semiconductors).
- High thermal conductivity of 0.54 $Wcm^{-1}K^{-1}$ (compared to 0.5 for GaAs).
- The largest exciton binding energy of semiconductors 60 meV (emissionslight excitonic stimulation up to 550K) [11].
- Drift mobilityμ saturates at higher fields and higher values than GaN (attractive for high frequency devices).
- A very high Shear Modulus (~45.5 GPa), indicating crystal stability.(Example:18.35GPa for ZnSe, 32.6 GPa for GaAs and 51.37 GPa for Si [12].
- UV detectors with maximum spectral response at 350nm [11].

### I.3.3. General properties of ZnO

#### I.3.3.1. Structural properties

Zinc oxide, known as zincite in its natural state, crystallizes in the compact hexagonal structure of the würtzite type, shown in **Figure I.3**, with the following lattice parameters:

$$a = 3{,}25\ \text{Å},\quad c = 5{,}12\ \text{Å}\ [13]$$

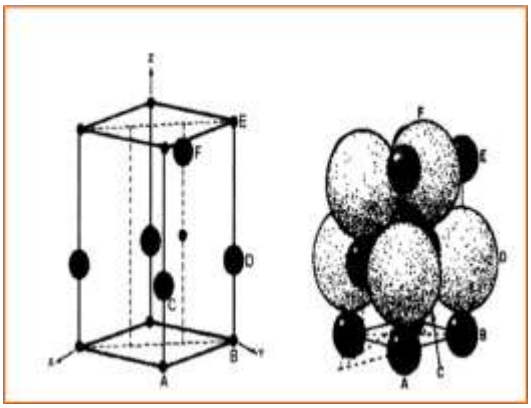

**Figure I.3.** Structure cristalline de l'oxyde de zinc [13].

Three different crystallographic phases are currently known as shown in **Figure I. 4** for zinc oxide: the Würtzite phase, the Blende phase and the Rocksalt phase. The Würtzite structure (hexagonal) is the thermodynamically most stable structure at room temperature; there Blende (cubic) structure is observed when ZnO is deposited on certain cubic symmetry substrates while Rocksalt structure is obtained when hydrostatic pressure (~10-15GPa) is applied to the Würtzite structure. The latter is a metastable phase that can persist at atmospheric pressure [14].

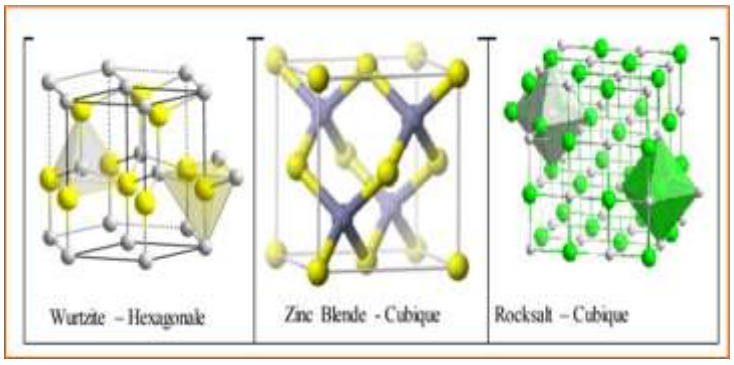




**Figure I.4.** Different structures of zinc oxide [14].

The piezoelectric behavior of ZnO, as well as other physical properties interesting, are due to the crystalline structure of this semiconductor, which can take three different structures, as shown in figure: Rocksalt, zinc blende and wurtzite.

Under ambient conditions, the thermodynamically stable phase is the structure wurtzite. The structure of zinc blende is on the contrary a metastable phase, which cannot bestabilized than in the case of growth on substrates of cubic symmetry. The lastphase, which is the rocksalt structure or Rochelle salt structure, can only be obtained by working at relatively high pressures. ZnO is also known aszincite in mineral form, and is very rare in nature [15]

- **The Würtzite phase of ZnO**

ZnO of compact hexagonal structure Würtzite, This structure consists oflayers of zinc atoms alternating with layers of oxygen $O^{2-}$ as shown in **Figure I.5**. The ZnO pitch lattice parameters under normal temperature and pressure conditions are given by: a=b=3.2499, c=5.2060 Å, α=β=90° and γ=120°,The volume of theunit cell is 47.58 $Å^3$[16].

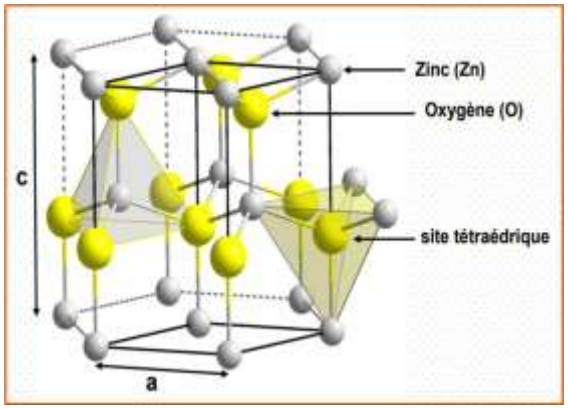




**Figure I.5.**Wurtzite Structure of Zinc Oxide [17].

### I.3.3.2.Optical properties

Zinc oxide is a transparent material, it is classified among the candidates which possess amazing optical properties which manifest themselves during the interaction of light (electromagnetic wave) with matter (the electrons of matter). For semiconductors: If an electromagnetic wave at low temperatures is capable to transfer electrons from the valence band (BV) to the conduction band (BC), that is to say, if this energy is at least equal to that of the width of the forbidden band, it is said that this wave is completely absorbed. We therefore expect to observe an absorption threshold that determines the width of the forbidden band, it is one of the methods used to calculate the gap. In the case of a direct gap semiconductor ZnO example, the photon energy is directly related to the width of the forbidden band by the following relation [18]:

$$Eg = h\upsilon \dots \dots \dots \dots . I.1$$

The optical properties of zinc oxide have been studied by several techniques. They concern the study of optical absorption, transmission, reflection, photoluminescence or the optical gap.

**Table I.1.** Some optical properties of ZnO [19].

| | |
|---|---|
| Dielectric constant | $\varepsilon_{//} = 8.7$<br>$\varepsilon_{\perp} = 7.8$ |
| Absorption coefficient | $10^4$ ($cm^{-1)}$ |
| Refractive index at 560 nm | 1.8-1.9 |
| Refractive index at 590 nm | 2.013-2.029 |
| Width of the excitonic band | 60 (meV) |

| | |
|---|---|
| Transmittance | >90% |

### I.3.3.3.Electrical properties

Zinc oxide is a type II VI semiconductor with a wide direct band gap of 3.37 ev at room temperature. This energy also called gap corresponds to that which causes an electron to pass from the band of valence (BV) to the conduction band (BC). ZnO exhibits an electrical conductivity natural type n which is due to the presence of interstitial zinc atoms. By varying the value of the conductivity by doping processes, the gap can go from 3.30 to 3.39 ev [20].

The electronic structure of the zinc and oxygen is [21]:

- **O : $1s^2\ 2s^2\ 2p^4$**
- **Zn: $1s^2\ 2s^2\ 2p^6\ 3s^2\ 3p^6\ 3d^{10}\ 4s^2$**

The 2p states of oxygen form the valence band and the 4s states of zinc constitute the conduction zone of the ZnO semiconductor.

**Table I.2.**Some electrical properties of ZnO [22].

| | |
|---|---|
| Nature of the for bidden band | Direct |
| Width of the band for bidden at 300°K | 3.37(ev) |
| Type of conductivity | N or P |
| Effective mass of electrons | 0.28 $m_0$ |
| Effective mass of holes | 0.6$m_0$ |
| Density of states in BC | 3.71 $10^{18}$ ($cm^{-3}$) |
| Density of states in BV | 1.16 $10^{19}$ ($cm^{-3}$) |
| Minimum resistivity | $10^{-1}$ (Ω. cm) |

| | |
|---|---|
| Maximum resistivity | $10^6$ (Ω. cm) |

### I.3.5. ZnO application

- **Photocatalysts**

Photocatalysis is used in general for air purification, water treatment it is also used in the discoloration of colored aqueous effluents, the elimination of odors and the self-cleaning coating of surfaces. This is made possible by the transfer and trapping of free charges to intermediate energy levels. The charges created migrate to the surface of the catalyst and react with adsorbed substances capable of accepting or donating electrons. The most widely used catalyst materials are semiconductors with a wide forbidden band, such as for example $TiO_2$, ZnO, ZnS and $SnO_2$ [23].

- **Gassensors** [24].
- **Organic solar cells**

. Zinc oxide is also being considered as a support material in solar cells. A nanostructured surface of ZnO as a support can increase the effective surface of the cell and improve the yield. It allows an efficient transport of photons to the active layer and it also has a good electrical conductivity which is required to obtain the least loss of transport of the photogenerated charges [24].

- **Intelligent glazing and anti-UV coating layers**

ZnO has the particularity of absorbing ultraviolet radiation while being transparent to visible light, hence its application as an anti-UV protective layer [23].

## I.4.Titanium dioxide

### I.4.1.History of $TiO_2$

Titanium (Ti) was discovered in 1791, in England, by William Gregor who identified this new element in the ilmenite mineral $FeTiO_2$ [25]. Titanium dioxide, also known as

titanium(IV) oxide or titania also known as Titania belongs to the family of transition metal oxides, chemical formula $TiO_2$ [26], relatively abundant in the earth's cheap and weekly toxic [25].

### I.4.2.Definition of $TiO_2$

$TiO_2$ is a white color as shown in **Figure I.6** found in all kinds of paints, printing ink, plastics, paper, synthetic fibers, rubber, condensers, painting colors and crayons, ceramics, electronic components along with food and cosmetics.

**Figure I.6.** Reagent-grade $TiO_2$ powder (anatase, 99% purit) [27].

$TiO_2$ is exists naturally in three crystalline forms; anatase, rutile and brookite as shown in **Figure I.7** [26].

A) Anatase B)Rutile C)Brookite

**Figure I.7.** Crystal forms of titanium dioxide [25].

### I.4.3. General properties of $TiO_2$

#### I.4.3.1. Structural properties

Titanium dioxide exists in many polymorphic forms of which ‘the rutile’ structure is the most common. Other naturally occurring forms are ‘anatase’, ‘brookite’. as shown in **Figure I.8** [28].

Anatase and brookite are meta-stable phases, and rutile is thermodynamically stable. Anatase and brookite $TiO_2$ irreversibly and exothermically converts to rutile at temperatures exceeding 600 °C [29].

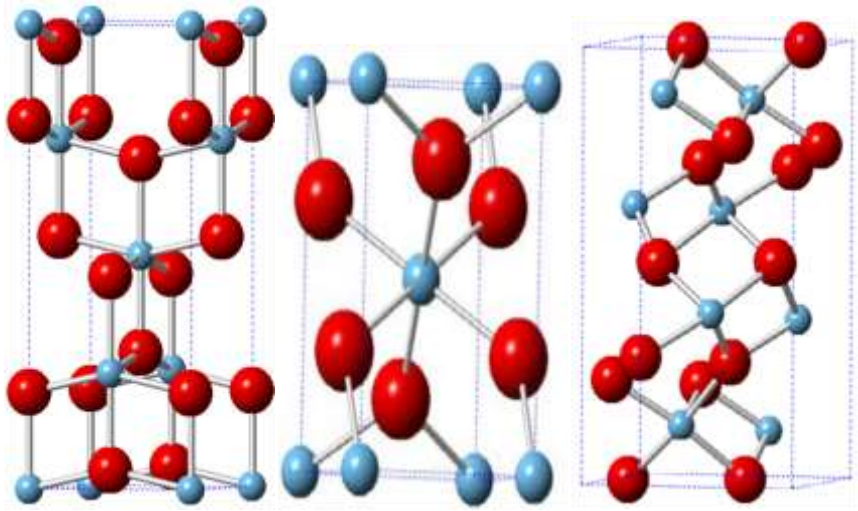

**A) Anatase** **B) Rutile** **C) Brookite**

**Figure I.8.** Crystal structure of $TiO_2$ A) Anatase, B) Rutile and C) Brookite [29].

The application of anatase phase or rutile phase depends on it is crystallinity and isomorphism.Therefore the application can vary. For example, the anatase phase is most used in charge separation devices, while rutile is predominantly used in gas sensors and dielectric layer [30].

### I.4.3.2. Optical properties

Titanium dioxide has a high refractive index *n* in the visible rang that averages values of 2.7 in rutile and 2.5 in anatase. The refractive index is a measure of the metal oxide’s ability to scatter photons. In this sense, rutile reflects light more efficiently compared to anatase and brookite, which marks rutile as an optimal pigment. Interestingly, the metal oxide has a dual behaviour towards light, by scattering and absorbing ultraviolet radiation, both highly desired properties in photocatalysis [27].

### I.4.3.3. Electrical properties

Titanium oxide appears as an n-type semicondictor and it is known excellent photocatalytic activity [31]. Rutile phase $TiO_2$ has a band gap of 3.02ev (411 nm), while anatase phase has aband 3.23ev (384nm) [32].

### I.4.4. $TiO_2$ Application

Like all transition metal oxides. Titanium dioxide ($TiO_2$) is a multifunctional material and can be used is many applications, both in the field of catalysis and in electronics or optics.

$TiO_2$ in powder form is widely used in heterogeneous photocatalysis because it is very stable, non-toxic, and efficient. These properties have made it occupy a distinct position among other oxides [33].

$TiO_2$ nanoparticles have multiple applications in cosmetics such as sunscreen, powder, eye shadow and deodorants (An antibacterial agent). Because he has the ability to absorb and reflect UV rays, opacifying ability, possibility of making a product transparent at diameters less than 30 nm [34].

**Table I.3.** Other $TiO_2$ applications [35].

| Domain | Applications | Properties |
|---|---|---|
| **Environment** | Wallpaper, paint, coatings, curtains, lampshades windows, cement,<br>Tunnel walls, lamps tunnels, soundproof walls air purifier, water disinfection used. | Self-cleaning<br>Antibacterial<br>Air purification<br>Water purification |
| **Medical** | Tiles, room walls of operations | Antibacterial<br>Sterilization |

| | | |
|---|---|---|
| | | Self-cleaning |
| **Energy** | Solar cells<br><br>Hydrogen production | Conversion of solar energy<br><br>Hydrolysis of water |

## I.5. Nanocomposites synthesis techniques « Sol-Gel »

### I.5.1. Historique of Sol-Gel

The sol-gel process was first used in 1845 for the polymerization of silicic acid $Si(OH)_4$ into solid glass under moist air. It took nearly a century for this idea to be applied in industry, and that by the german firm Schott Glaswerke, for the manufacture of glass containers. The first sol-gel patent was filed in 1939 [36]. For the production of automobile mirrors [37].

### I.5.2.Sol- gel method

Sol- gel method is a bottom up [2], and it is mean transition from a liquid "sol" (colloidal solution) into a "gel" phase. Usually inorganic metal salts or metal organic compounds such as metal alkoxide are used as precursors. A colloidal suspension or a "sol" is formed after a series of hydrolysis and condensation reaction of the precursors. Then the sol particles condense into a continuous liquid phase (gel).

Three reactions are used to describe the sol-gel process: hydrolysis, alcohol condensation and water condensation. The two phases which describe the sol-gel process are defined as follows:

- Sol: a stable suspension of colloidal solid particles or polymers in a liquid.
- Gel: porous, three-dimensional, continuous solid network surrounding a continuous liquid phase [38].

Generally, we can say that the sol-gel process takes place in these major steps as shown in **Figure I.9**.

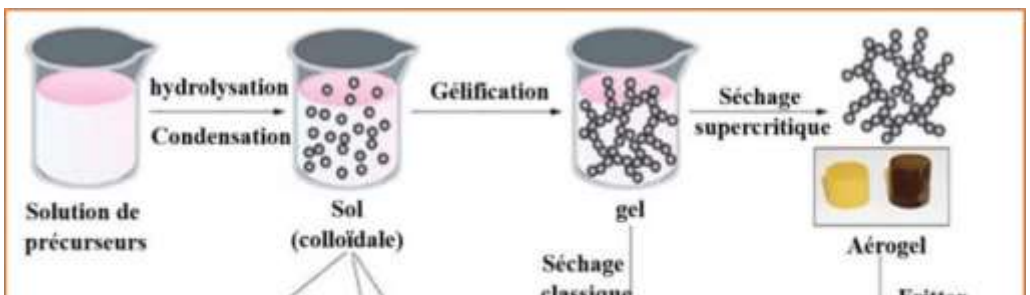

### I.5.3. Reaction mechanisms of the sol-gel method

#### I.5.3.1. Hydrolysis reaction

The hydrolysis of a substance is its decomposition by water thanks to the H+ and OH ions coming from the dissolution of water. So this is the substitution nucleophile of an –OH ligand by an –OR ligand. This reaction is accompanied by aconsumption of water and a release of alcohol it is the hydroxyl groups(R-OH) as shown by the following chemical reaction [39]:

$$M(OR)_n + H_2O \longrightarrow (OR)_{n-1}\text{-}M\text{-}OH + R(OH) \quad \ldots\ldots \text{ I.2}$$

#### I.5.3.2. Condensation reaction

The groups (HO-M $(\text{-OR})_{n-1}$) generated during hydrolysis react either with each other giving a molecule of water (reaction 2), or with a molecule of the alkoxide M(-OR) ingiving an alcohol molecule (reaction 1) thus resulting in the creation of M-O-M bridges oreach oxygen atom becomes a bridge connecting two atoms of the metal M. This leads to the formation of a gel whose viscosity increases over time, this gel contains solvents and precursors that have not yet reacted.

This process is governed by the following reactions at room temperature:

$$(OR)_{n-1}\text{-M-OH} + \text{RO-M-}(OR)_{n-1} \rightarrow (OR)_{n-1}\text{- M-O-M-}(OR)_{n-1} + \text{R-OH}\ldots\ldots\text{I.3}$$

$$(OR)_{n-1}\text{-M-OH} + \text{HO-M-}(OR)_{n-1} \rightarrow (OR)_{n-1}\text{- M-O-M-}(OR)_{n-1} + H_2O\ldots\ldots\ldots\text{I.4}$$

### I.5.3.3. The sol-gel transition

When all the bonds have been used, the gel is formed. From a macroscopic point of view, the transition can be followed by the mechanical behavior of the solution. It then results in the divergence of the viscosity of the solution and a growth of the elastic constant in the gel phase G. The evolution of the viscosity of a sol and that of its Coulomb modulus are thus presented schematically in the **Figure I.10**, as a function of time: at the complete formation of the gel, the viscosity becomes infinite, while the elastic constant tends towards its maximum value [40].

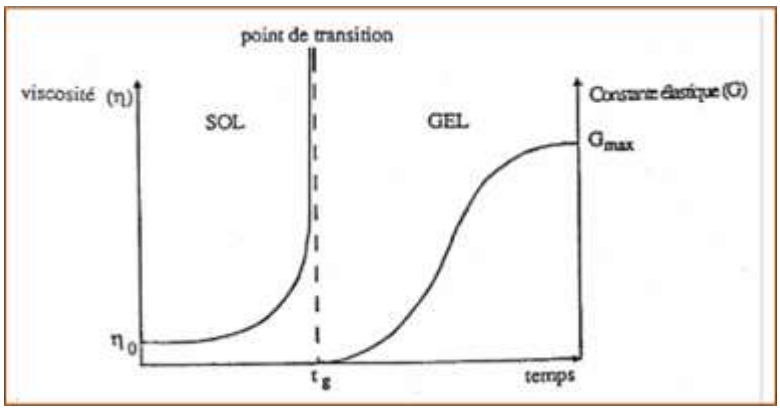


**Figure I.10.** Evolution of the viscosity of the solution and of the elastic constant of the gel; tg is the time after which the sol-gel transition is reached [40].

### I.5.3.4. Gel aging

Once the gel has formed, the system continues to evolve by progressive fixation of the free species. At room temperature this phenomenon can last for months depending on the pH, the temperature and the composition of the gels [41].

### I.5.3.5. Drying

This operation consists in eliminating the water (or the solvent) contained in the pores of the solid and possibly the physisorbed water.

In general, evaporative drying risks densifying the gel and even cracking it, in particular because of the appearance of strong capillary tensions resulting from the presence of

a liquid-gas interface. The appearance of this interface can be annihilated by following drying by sublimation (freeze drying) or drying under the supercritical conditions of the interstitial solvent (supercritical drying).

The gels are in the form of a nanoporous three-dimensional solid network delimiting pores filled with solvent. A difficulty of the drying phase is the extraction of the solvent by air without modifying the nanostructured porosity of the gels.Supercritical drying makes it possible to obtain a dry material with low thermal conductivity (less than 0.015 W $m^{-1}$ $K^{-1}$) [42].

**A. Xerogels**

This type of material is obtained when the soil undergoes pressure dryingatmospheric and at room temperature or slightly above. The product thus prepared has a porous texture. This method has the characteristic main to generate a possible collapse of the texture during evaporationsolvents.

**B. Aerogels**

To remedy the problem of material contraction during drying atroom temperature and at atmospheric pressure, it is possible to circumvent the critical point of the solvent. The aerogels produced by this method are characterized bya very high porosity that can reach 90%, hence a very low density. Moreover the structure of the network of the gel is preserved. This method requires working with high temperatures and pressures [43].

**I.5.3.6. Calcination**

The purpose of this operation is to transform a mixture of calcined powders into a powder having a well-defined composition and crystalline structure. This powder is subjected to a thermal cycle under controlled atmosphere, which leads to solid phase diffusion phenomena, and consequently the formation of the desired phase.

The calcination treatment was carried out in a controlled muffle furnace programmable type Oven (Wisd) its maximum temperature is 1200°C, in temperature 300°C until 2 hours [44].

**I.5.5. Advantages and disadvantages of the sol-gel method**

**I.5.5.1. The main advantages of the sol-gel method**

- ✓ Ease of implementation.
- ✓ The purity of the material obtained, thanks to the purity of the precursors and the elimination of organic residues.
- ✓ The many achievable textures (powders, fibers, monoliths, and thin layer) with specific properties.
- ✓ The process is done at low temperature or close to room temperature.
- ✓ The possibility of doping in the ground phase.
- ✓ The possibility of having homogeneous and stoichiometric materials.
- ✓ Realization of multi-component deposits in a single operation.
- ✓ Deposition of thin layers on both sides of the support in a single operation [18].

### I.5.5.2. Disadvantages of the sol-gel process

Like any synthesis process, the sol-gel has some disadvantages, including main are:

- ✓ Cost of high - alkoxide precursors.
- ✓ Manipulation of a large amount of solvents [21].

## I.6.An overview of photocatalysis

### I.6.1. Definition of photocatalysis

The photocatalysis was discovered in 1972 by Fujishima and Honda, and is a natural phenomenon in which a substance, the photocatalyst, initiates a chemical reaction through the action of light, without degrading itself [37].

We can distinuish different types of catalysis according to the nature of the catalyst:

- ❖ Homogeneous catalyst where catalyst and reactants are in the same phases.
- ❖ Heterogeneous catalysis where catalyst and reactants from several phases [45].

### I.6.2. Principe and mechanism of heterogeneous photocatalysis

Photocatalysis relies on semiconductors as catalysts because of their band gap, including ($TiO_2$, ZnO, $WO_3$, $SnO_2$ ……etc). The latter is few ev and separates the occupied band from higher energy called valence band (BV) of the conduction band (BC) vacuum in the ground state. The principle of photocatalysis is based on the generation of photoelectrons ($e^-$)

in the conduction band and holes ($h^+$) in the valence band of the semiconductor (SC) after exposure to light wavelength greater than or equal to the band gap energy. The $e^-$ loads/$h^+$ migrate to the surface of the semiconductor where they serve as sites redox for the destruction of adsorbed pollutants. **Figure I.11** shows how oxidative species are generated when a photocatalyst is irradiated by a light of energy hυ>Eg and their mode of action on water and pollutants.

Here we give the main reactions that take place:

$$\text{Semiconductor} + h\upsilon \rightarrow h^+ + e^- \ldots\ldots \text{I. 5}$$

Holes react with water and organic pollutants adsorbed on the surface of the semiconductor, according to the reactions:

$$H_2O + h_{BV}^+ \rightarrow HO^- + H^+ \ldots\ldots \text{I. 6}$$

$$\text{pollutant} + h_{BV}^+ \rightarrow \text{pollutant}^+ \ldots\ldots \text{I. 7}$$

The hydroxyl radicals formed also participate in the degradation of pollutants [46]:

$$\text{pollutant} + HO^- \rightarrow CO_2 + H_2O \ldots\ldots \text{I. 8}$$

## I.7. Conclusion

In this chapter, we have presented a bibloigraphic study on the structural, optical, and electrical properties of zinc oxide (ZnO) and titanium dioxide ($TiO_2$) and their applications. Also we have exposed an overview of the Sol-Gel technique and finally we have given a simple definition of photocatalytic.

**References**

[1] S.R.Miro, Synthesis and Characterization of Magnetic Nanocomposites and Their Applications Study, thèse de doctorat, Université Autònoma de Barcelona, UAB, (2017), p 17-18.

[2] W.S. Khan[1], N.N. Hamadneh[2], W.A. Khan[*1], Science and applications of Tailored Nanostructures, Polymer nanocomposites – synthesis techniques, classification and properties, (2016), p 52-64.

[3] C.C. Okpala, Nanocomposites– An Overview, International Journal of Engineering Research and Development, 8 (2013), p 18.

[4] https://en.wikipedia.org/wiki/Nanocomposite 30/4/2023 23:45

[5] S. Pandya, Nanocomposites and its application-review, Research gate, (2015).

[6] M.M. Ali, M.J. Haque, M.H, Kabir, M.A. Kaiyum, M.S Rahman, Nano synthesis of ZnO-$TiO_2$ composites by sol-gel method and evaluation of their antibacterial, optical and photocataylytic activities, 11(2021),100199.

[7] N. Hellen, H. Park, K.N. Kim, Characterization of ZnO/$TiO_2$nanocomposites prepared via the Sol-gel method, Journal of the korean ceramic society , 44 (2018)p 140.

[8] R. Ghomri, Étude des propriétés de l'oxyde de zinc non dopé et dopé, Thèse de doctorat, Université Badji Mokhtar Annaba,Algérie, (2017) ,p 3.

[9] A. Benaboud, Etude des propriétés optiques, morphologiques, et photocatalytiques des couches minces de l'oxyde zinc « ZnO » dopé au Fer ,thèse de doctorat , Université Larbi Ben M'hidi, Oum El Bouaghi, Algérie, (2018),p 5.

[10]S. Hamdelou, Préparation et étude électrique de poudres nanocristallines de ZnO pur et dopé par différents oxydes, thèse de doctorat ,Université Mentouri-Constantine Algérie, (2017),p 16.

[11] S. Abed, Elaboration et Caractérisation de Couches minces d'Oxyde de Zinc Obtenues par Spray Pyrolyse, mémoire de magister, Université Mentouri Constantine, Algérie, p 9.

[12] E.H. Benyahia, Caractérisation structurale et optique de couches minces formées par des agrégats des nanocristaux de ZnO, mémoire de magister, Université Mentouri Constantine,Algérie, p 5.

[13] A. Moustaghfir, Élaboration et caractérisation de couches minces d'oxyde de zinc. Application à la photoprotection du polycarbonate, thèse de doctorat, Université Blaise Pascal - Clermont-Ferrand II, France, (2004),p 13 ;14.

[14] A. Herzi, Elaboration et caractérisation des couches minces du semi-conducteur ZnO non dopé et dopé par l'Argent, thèse de doctorat, Université Freres Mentouri – Constantine 1,Algérie, (2020), p 5 ;6.

[15] B. Rahal, Elaboration et Caractérisation des Couches minces du Semiconducteur ZnO pures et dopées par le Cadmium, thèse de doctorat, University Freres Mentouri – Constantine 1, Algérie, (2017), p 8.

[16] S. Harouni, Elaboration et étude des propriétés physiques et chimiques de nanopoudres d'oxyde de zinc pour une application en photocatalyse hétérogène, thèse de doctorat, University Freres Mentouri – Constantine 1, Algérie, (2020), p 11-12.

[17] A. Mahroug, Etude des couches minces d'Oxyde de Zinc dopé Aluminium et Cobalt élaborées par la technique sol gel-spin coating. Application à la photodétectionet au photocourant, thèse de doctorat, University Freres Mentouri – Constantine, Algérie, (2015),p.31.

[18] S. HAYA, Etude des propriétés structurales et optiques de nano-cristaux semi-conducteurs à grand gap synthétisés par voie sol-gel modifiée, mémoire de magister, Université Mentouri Constantine, Algérie, (2010), p 16 ; 58-59.

[19] S. Benramache, Elaboration et caractérisation des couches minces de ZnO dopées cobalt et indium, thèse de doctorat, Université Mohamed Khider – Biskra, Algérie, (2012), p 13.

[20] M. Khammar, Etude de L'influence d'un spray pyrolytique sur les caracteristiques de couches minces de ZnO, thèse de doctorat, University Freres Mentouri – Constantine 1, Algérie, (2017), p 8.

[21] M. Dahnoun, Preparation and characterization of Titanium dioxide and Zinc oxide thin films via Sol-Gel (spin coating) technique for optoelectronic applications, thèse de doctorat, University Mohamed Khider of Biskra, Algérie, (2019/2020), p11;49.

[22] A. Elkaiem, Contribution au développement des matériaux nano-composites à base de ZnO et polymère étude structural et optique, mémoire magister, Université Constantine, Algérie, (2015).

[23] H. Bozetine, Synthèse des nanostructures de ZnO par la méthode hydrothermale et leurs applications, thèse de doctorat, Université Mouloud Mammeri TiziOuzou, Algérie, (2017), p 19-20 ; 14.

[24]S. Khodja ,Elaboration et caractérisation de couches minces de ZnO pour des applications optoélectroniques ,thèse de doctorat, Université Badji Mokhtar- Annaba, Algérie, (2017), p 31-32 ;33-34.

[25] F. Hanini, Etude des propriétés physiques de couches minces$TiO_2$ élaborées par différentes techniques, thèse de doctorat, université constantine 1, Algérie, (2014), p 3.

[26] A.J. Haider, Z.N. Jameel, I.H.M. Al-Hussaini, Review on : Titanium dioxide applications, Energy Procedia,157 (2019), p 17-29.

[27] J. Environ, Review on: Titanium Dioxide: Structure, Impact, and Toxicity, 19 (2022), p 1-2.

[28] K.M. Glassford, J.R. Chelikowsky, Structural and electronic properties of titanium dioxide, Physical Review B, 46 (1992) 1284.

[29] V. Etacheri, C.d. Valentin, J. Schneider, D. Bahnemann, S.c. Pillai, Visible-Light Activation of $TiO_2$Photocatalysts: Advances in Theory and Experiments, Journal of photochemistry and photobiology C: photochemistry reviews, 25, (2015), p 6-7.

[30] J.V. Hernandez, Structural and Morphological modification of $TiO_2$ doped metal ions and investigation of photo-induced charge transfer processes, thèse de doctorat, Université du Maine, México, (2017), p 7.

[31] T.Shokuhfar, Structural and surface property characterization of titanium dioxide nanotubes for orthopedic implants, doctoral thesis, Michigan technological University, United States , (2010), p 18.

[32] R.Azouani, Elaboration de nouveaux nanomatériaux photocatalytiques actifs sous rayannement visible, thèse de doctorat, Université paris 13, France, (2009), p 6.

[33] J. Guillot, Couches minces d'oxynitrure de titane : la réactivité comme moyen original de caractérisation physico –chimique, thèse de doctorat, Université de Bourgogne, France, (2002), p 8.

[34] L. Daragnes, Les nanoparticules de dioxyde de titane, leur place dans l'industrie cosmetique et ses dangers, Thèse de Doctorat, Université de bordeaux, France, (2018).
[35] S. bouhadoun, synthèse de nanoparticules de dioxyde de titane par pyrolyse laser et leur application en photocatalyse, thèse de doctorat, université paris –saclay, France, (2015), p 25.

[36] N. Bou Orm, Nano-matériaux hybrides pour l'élimination de micro-polluants organiques (HAP) dans les effluents aqueux, thèse de doctorat, Université de Claude Bernard - Lyon I, France, (2012), p 39.
[37] S. Abbad**,** Etude de l'effet du dopage et des paramètres de synthèse de poudres nanocristallines de $TiO_2$ préparées par sol-gel sur les propriétés physiques et photo-catalytiques, Thèse de doctorat, Université Larbi Ben M'hidi, Algérie, (2022), p 32;34 ;39.
[38] R. Messemche, Elaboration and characterization of undoped and doped titanium dioxide thin layers by sol gel (spin coating) for photocatalytic applications, doctoral thesis, University Mohamed Khider of Biskra ,Algérie, (2021), p 31.
[39] F. Mahcene, Synthèse par Sol-gel et caractérisation structurale et optique de nano poudres de ZnO pures et dopées en Aluminium (0.1, 0.5 , 0.75 , 1 , 5 , 7,10,15 et 20 % at ), thèse de doctorat, Université Mentouri Constantine 1,Algérie, (2021), p 32-33.

[40] M.S. Rabaste, Microcavités optiques élaborées par voie sol-gel : applications aux ions terre rare d'$Eu^{3+}$ et aux nanocristaux semiconducteurs de CdSe, thèse de doctorat, Université Claude Bernard - Lyon 1, France, (2003), p 38-39.

[41] A. Marouani, Etude des caractéristiques physiques de couches minces à base d'oxydes métalliques déposés par voie sol-gel, thèse de doctorat, Université Ferhat Abbas –setif-1, Algérie, (2018), p 75.

[42] S. Bouzebboucha, Synthèse d'oxyde de titane par le procédé sol gel. Leur application en massif et en couche mince, mémoire de magister,Université 08Mai 1945 Guelma, Algérie, (2010), p 16.

[43] D. Adnane, Caractéristiques Optiques Et Structurales Des Couches Minces D'oxyde De Titane Obtenues Par Voie Sol-gel, mémoire de magister, Université de Constantine, Algérie, (2005), p 32.
[44] A. Mebarek, Elaboration et caractérisation de céramiques $ZnO{-}TiO_2$, thèse de doctorat, Université Badji Mokhtar Annaba, Algérie, (2018), p 29.

[45] T. Martinez, Revêtements photo-catalytiques pour matériaux de construction: formulation, évaluation de l'efficacité et écotoxicité, thèse doctorat, Université Toulouse III – Paul Sabatier, France, (2012), p 19.

[46] M.A. Brik, Elaboration et caractérisation de couches de conversion de longueur d'ondes à base de matériaux dopés terres rares en vue d'applications énergétiques, thèse de doctorat, Université Saad Dahlab de Blida 1, Algérie, (2021), p 55,56.

# Chapter II

## Preparation and characterization methods

## II.1.Introduction

In this chapter we describe, firstly, the preparation steps of the nanocomposites based on Zinc oxides (ZnO) and titanium dioxide ($TiO_2$) by Sol-gel method. Then, we detail the techniques used for the characterization which are; X-ray diffraction (XRD), Fourier transform infrared spectroscopy (FTIR) and UV-Visible (UV-Vis) spectroscopy. Finally, we define the exprimental protocols used to carry out the photocatalytic test.

## II.2. Synthesis of the nanocomposites based on ZnO and $TiO_2$ by the Sol-gel method

### II.2.1. Chemical products used

In order to prepare ZnO/$TiO_2$by the Sol-gel method, we used the chemical products shown in **table II.1.**

**Table II.1.** Caracteristics of the chemical products used :( structure, molar mass, purity, infusion temperature and supplier).

| Name | Zinc oxide | Titanium dioxide | Citric acide | Ethanol |
|---|---|---|---|---|
| **Chemical structure** | ZnO | $TiO_2$ | $C_6H_8O_7$ | $C_2H_6O$ |
| **Molar mass (g/mol)** | 81.38 | 79.86 | 192.12 | 46.08 |
| **Degree of purity (%)** | 99.99 | 99 | - | 96 |
| **Infusion temperature(°C)** | 1975 | 1855 | 153 | -114 |
| **Supplier** | Riedel-de Haen | Sigma-Aldrich | Junssen | Biochem chemopharma |

| Picture | | | | |
|---|---|---|---|---|
| |  |  |  |  |

### II.2.2. Equipments used

The device we used to accomplish this work are shown in **table II.2**.

**Table II.2.** Characteristics of the devices used (descriptions and pictures)

| Devices used | Description | Picture |
|---|---|---|
| **Electric scale (KERN)** | Display accuracy $10^{-4}$g, and its maximum range 150 g |  |
| **A magnetic stirrer** | A magnetic stirrer or magnetic mixer is a laboratory device that employs a rotating magnetic field to cause a stir bar (or *flea*) immersed in a liquid to spin very quickly, thus stirring it. |  |

| | | |
|---|---|---|
| **A thermometer** | Measure the temperature of the solution the maximum temperature is limited to 250 °C |  |
| **Oven (Wisd)** | Its maximum temperature is 1200 °C. |  |
| **Mortar and pestle** | A ceramic pestle and mortar for milling powder. |  |
| **UV Lamp (Eurl Aquapure)** | Capacity = 14 W |  |
| **Centrifuge (Osterode/Harz)** | VA max = 60 Volt |  |

| | | |
|---|---|---|
| **PH meter (Jenway)** | Measure the ph of the solution, indicating its acidity or a ikalinity expressed as PH.<br>Measure the temperature of the solution. |  |
| **Spectrophotometer (SECOMAM PRIM)** | The spectral range is[330 nm - 900 nm ] |  |

### II.2.3. Preparation of ZnO/$TiO_2$ nanocomposites

Sol-gel method was used to prepare our samples, zinc oxide and titanium dioxide were used as precursors to prepare the solution.

The deposition process takes place inside a metal chamber (fume hood) where the toxic gases are released through this high exhaust. The assembly includes a beaker containing the deposition solution, a heating plate resistance used to heat the solution, a magnetic stirrer equipped with a button to guarantee the stirring and to control the speed of this inside the solution by rotating the latter.

In the first stage, a solution (Ethanol+ distilled water) was prepared, and then an amount of ZnO and $TiO_2$ was added according to the work. Then we leave it under continuous stirring for (30 minutes to an hour) as shown in **Figure II.1.A.**

In the second stage, we prepare the fixing solution (Citric acid+ distilled water) and leave it until it becomes homogeneous as shown in **Figure II.1.B**. Then we add it to the first solution and leave it under stirring for (15 minutes) at temperature of 65 °C, to obtain a gel solution as shown in **Figure II.1.C.**

In the third stage, we introduce the gel solution into the electric oven at 300°C for 5 minutes as shown in **Figure II.1. D.**

In the end we get a powder that we mill with a mortar as shown in **Figure II.1.E.**

We have summarized the preparation of ZnO-$TiO_2$ Nano composites by diagram as shown in **Figure II.2**

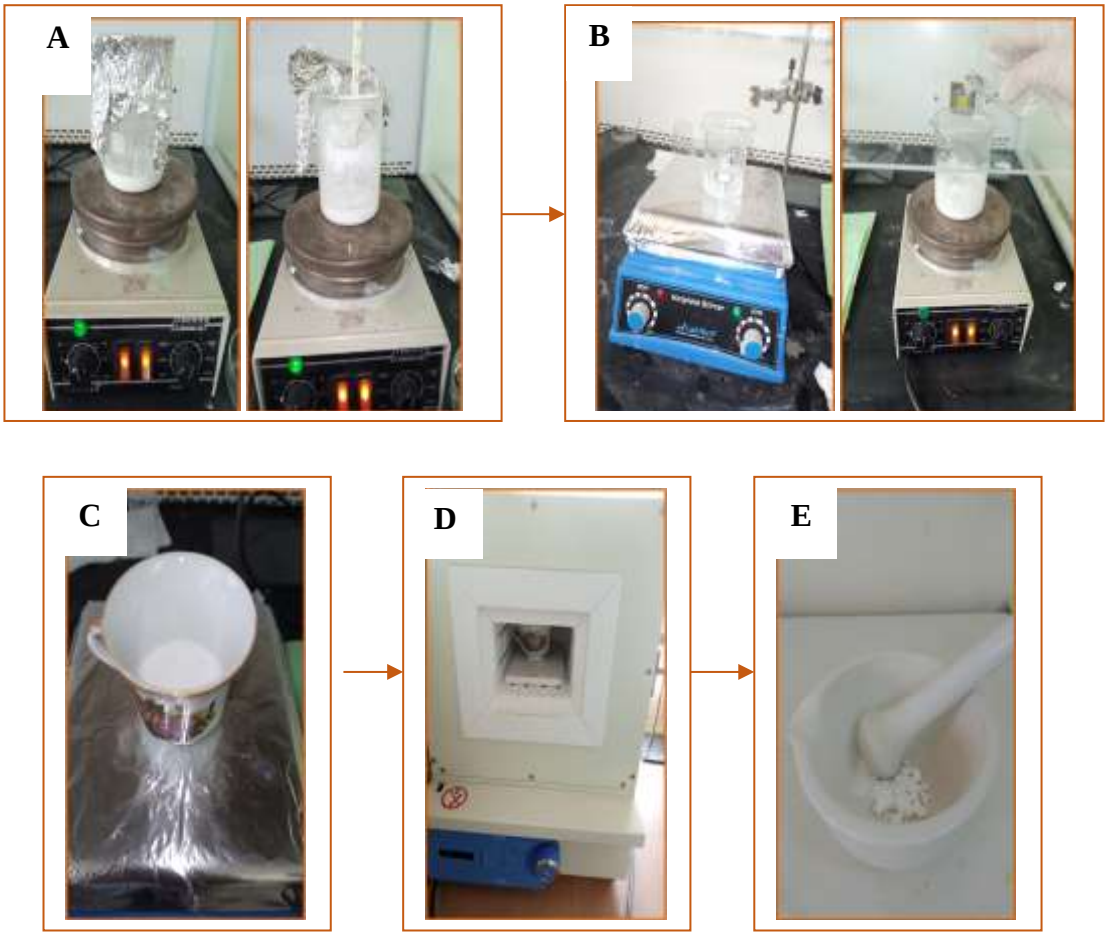


**Figure II.1.** Preparation steps of a nanocomposite based on ZnO and $TiO_2$.

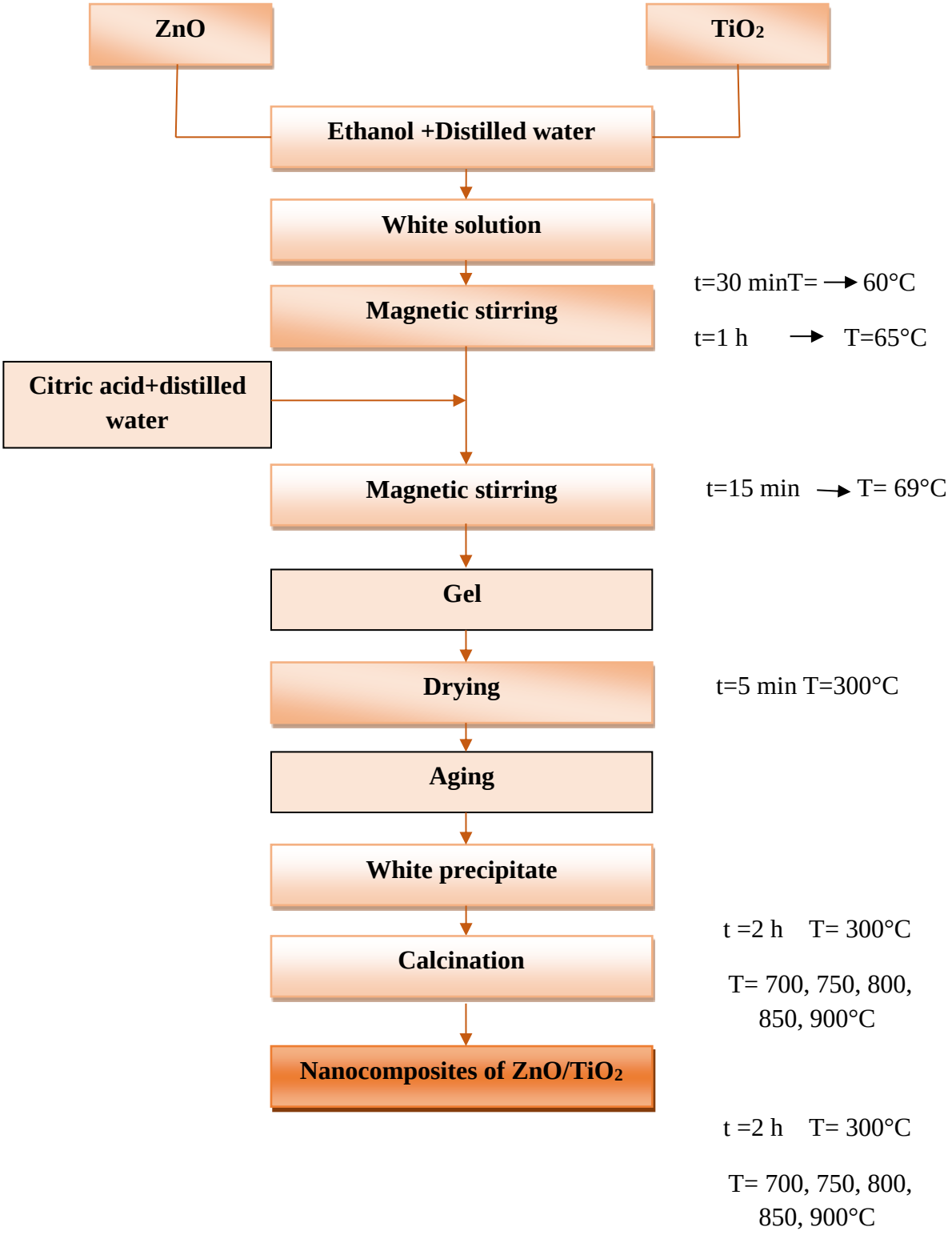


**Figure II.2**. Synoptic diagram shows the preparation steps of $ZnO/TiO_2$ nanocomposites by the sol gel method.

Two sets (series) of samples were prepared:

- **The first series:** we varied the composition of ZnO and $TiO_2$ to obtain the nanocomposites of ZnO/$TiO_2$.

  ZnO percentages are: 85%, 80%, 75% and 65%, $TiO_2$ percentages are 15%, 20%, 25% and 35%; As shown in **Table II.3.**

  The different samples with the different percentages are:

  85%ZnO/15%$TiO_2$, 80%ZnO/20%$TiO_2$, 75%ZnO/25%$TiO_2$, 65%ZnO/35%$TiO_2$, these samples are calcinated at a low temperature of 300°C, the calcination time is two hours,as shown in **Figure II.3.**

**Figure II.3.** The powder obtained (85%ZnO/15%$TiO_2$, 80%ZnO/20%$TiO_2$, 75%ZnO/25%$TiO_2$ and 65%ZnO/35%$TiO_2$)

**Table II.3.** The exprimental conditions of calcination.

| Samples | Calcination Temperature (°C) | Calcination Time | Device Used |
|---|---|---|---|
| 85%ZnO/15%$TiO_2$, | 300 | two hours | Oven Wisd |
| 80%ZnO/20%$TiO_2$, | 300 | two hours | Oven Wisd |
| 75%ZnO/25%$TiO_2$, | 300 | two hours | Oven Wisd |
| 65%ZnO/35%$TiO_2$, | 300 | two hours | Oven Wsid |

- **The second series :** This series presents the 80%ZnO/20%$TiO_2$ sample with different calcination temperatures (700,750, 800, 850, 900°C) and a sample without calcination , the calcination time is two hours as shown in **Table II.4** and **Figure II.4.**

**Figure II.4.** The nanocomposite obtained 80%ZnO/20%$TiO_2$ (with calcination at 300, 700,750, 800, 850 and 900°C)

**Table II.4.** The exprimental conditions of calcination.

| Sample | Calcination Temperature (°C) | Calcination Time | Device Used |
|---|---|---|---|
| 80%ZnO/20%$TiO_2$ | 700 | two hours | Oven wsid |
| 80%ZnO/20%$TiO_2$ | 750 | two hours | Oven wsid |
| 80%ZnO/20%$TiO_2$ | 800 | two hours | Oven wsid |
| 80%ZnO/20%$TiO_2$ | 850 | two hours | Oven wsid |
| 80%ZnO/20%$TiO_2$ | 900 | two hours | Oven wsid |

## II.3. Characterization methods

In the following we give a brief idea of the characterization techniques used

### II.3.1. X-ray diffraction (XRD)

X-ray diffraction is a simple technique, easy to implement and not destructive. It provides information on the structural characteristics and microstructural such as: the existing phases and their proportions, the structure crystalline, the grain size and the rate of microdeformations [1].

#### II.3.1.1. principle of operation

X-ray diffraction occurs when the Bragg condition (equation II.1) is fulfilled. For a incident X-radiation of wavelength this condition meets [2]:

$$2d.\sin\theta = n\lambda \ldots\ldots \text{II.1}$$

Θ : incident angle between the ray and the sample plane.

λ : wavelength of the radiation

n : network order (integer)

d : inter-reticular distance between two crystallographic planes.

During an analysis by this technique, a beam of X-rays, emitted by a source, is sent to the sample to by analyzed under a angle Θ as shown in **Figure II.5**, and a detector receives the X – ray beam diffracted by this sample and records its intensity as a function of the diffraction angle 2Θ. When Bragg's law is verified, a diffraction peak corresponding to the family of planes considered is obtained on the diffractogram [3].

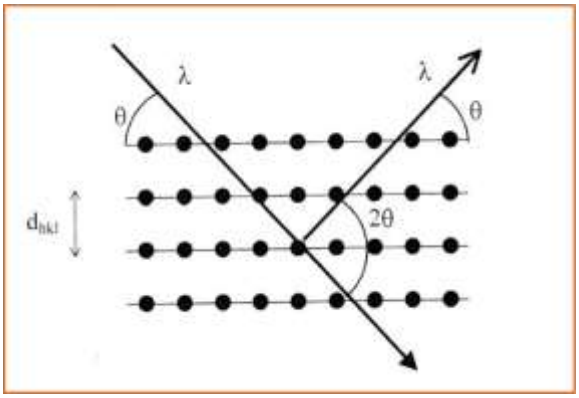


**Figure II.5.** Diagram representing the principle of X-Ray diffraction [3].

### II.3.1.2Determination of the cristallite size

The size of the crystallites can be calculated using the Scherrer's formula:

$$D = \frac{0.9\lambda}{\beta\cos\theta} \dots\dots\dots \text{II. 2}$$

Where, λ is the wavelength of the x-ray and $\beta$ is the full width at half maximum intensity in radians [4].

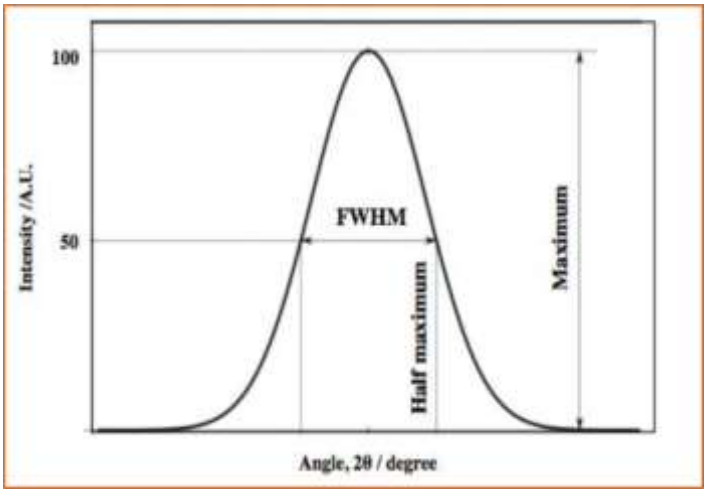


**Figure II. 6.** Illustration of the peak widths FWHM ($\Delta\theta$=$\beta$) [4].

### II.3.1.3. Experimental apparatus

As part of our study, we performed of XRD by the device : Thermofisher EQUINOX 100 as shown in **Figure II.7**, which is existing in the materials and structure of electromechanical systems and their reliability laboratory (LMSESR). The X-rays were produced from a source of CuKα, having a wavelength equal to 1,5406Å.

**Figure II.7.** Diffraction device of X-rays of type Thermofisher.

- **The diffraction peaks are defined using the JCPD files 00-036-1451 Zinc Oxide and 00-025-1164 Zinc Titanium Oxide obtained from the Highscore plus software as shown in Table II.5 and Table II.6.**

**Table II.5.** The diffraction peaks are defined using the JCPD files 00-036-1451 Zinc Oxide 00-025-1164 obtained from the Highscore plus software

| No | h k l | d[Å] | 2Θ[deg] | I[%] |
|---|---|---|---|---|
| 1 | 1 0 0 | 2.81430 | 31.770 | 57.0 |
| 2 | 0 0 2 | 2.60332 | 34.422 | 44.0 |
| 3 | 1 0 1 | 2.47592 | 36.253 | 100.0 |
| 4 | 1 0 2 | 1.91114 | 47.539 | 23.0 |
| 5 | 1 1 0 | 1.62472 | 56.603 | 32.0 |

| | | | | |
|---|---|---|---|---|
| 6 | 1 0 3 | 1.47712 | 62.864 | 29.0 |
| 7 | 2 0 0 | 1.40715 | 66.380 | 4.0 |
| 8 | 1 1 2 | 1.37818 | 67.963 | 23.0 |
| 9 | 2 0 1 | 1.35825 | 69.100 | 11.0 |
| 10 | 0 0 4 | 1.30174 | 72.562 | 2.0 |
| 11 | 2 0 2 | 1.23801 | 76.955 | 4.0 |
| 12 | 1 0 4 | 1.18162 | 81.370 | 1.0 |
| 13 | 2 0 3 | 1.09312 | 89.607 | 7.0 |
| 14 | 2 1 0 | 1.06384 | 92.784 | 3.0 |
| 15 | 2 1 1 | 1.04226 | 95.304 | 6.0 |
| 16 | 1 1 4 | 1.01595 | 98.613 | 4.0 |
| 17 | 2 1 2 | 0.98464 | 102.946 | 2.0 |
| 18 | 1 0 5 | 0.97663 | 104.134 | 5.0 |
| 19 | 2 0 4 | 0.95561 | 107.430 | 1.0 |
| 20 | 3 0 0 | 0.93812 | 110.392 | 3.0 |
| 21 | 2 1 3 | 0.90694 | 116.279 | 8.0 |
| 22 | 3 0 2 | 0.88256 | 121.572 | 4.0 |
| 23 | 0 0 6 | 0.86768 | 125.188 | 1.0 |
| 24 | 2 0 5 | 0.83703 | 133.932 | 3.0 |
| 25 | 1 0 6 | 0.82928 | 136.521 | 1.0 |
| 26 | 2 1 4 | 0.82370 | 138.513 | 2.0 |
| 27 | 2 2 0 | 0.81247 | 142.918 | 3.0 |

**Table II.6.** The diffraction peaks are defined using the JCPD files 00-036-1451 Titanium Oxide 00-025-1164 obtained from the Highscore plus software

| No | h k l | d[Å] | 2Θ[deg] | I[%] |
|---|---|---|---|---|
| 1 | 1 1 1 | 4.89000 | 18.127 | 4.0 |
| 2 | 2 2 0 | 2.99300 | 29.828 | 35.0 |
| 3 | 3 1 1 | 2.55200 | 35.137 | 100.0 |
| 4 | 2 2 2 | 2.44400 | 36.743 | 4.0 |
| 5 | 4 0 0 | 2.11500 | 42.718 | 13.0 |
| 6 | 4 2 2 | 1.72700 | 52.979 | 11.0 |
| 7 | 5 1 1 | 1.62700 | 56.517 | 30.0 |
| 8 | 4 4 0 | 1.49580 | 61.992 | 30.0 |
| 9 | 5 3 1 | 1.43050 | 65.161 | 1.0 |
| 10 | 6 2 0 | 1.33770 | 70.317 | 3.0 |
| 11 | 5 3 3 | 1.29010 | 73.323 | 6.0 |
| 12 | 6 2 2 | 1.27580 | 74.282 | 2.0 |
| 13 | 4 4 4 | 1.22140 | 78.199 | 1.0 |
| 14 | 6 4 2 | 1.13060 | 85.894 | 4.0 |
| 15 | 7 3 1 | 1.10130 | 88.765 | 9.0 |
| 16 | 8 0 0 | 1.05760 | 93.496 | 2.0 |
| 17 | 6 6 0 | 0.99710 | 101.165 | 2.0 |
| 18 | 7 5 1 | 0.97690 | 104.094 | 5.0 |
| 19 | 6 6 2 | 0.97060 | 105.053 | 1.0 |
| 20 | 8 4 0 | 0.94570 | 109.082 | 1.0 |

| | | | | |
|---|---|---|---|---|
| **21** | **6 6 4** | **0.90190** | **117.318** | **1.0** |
| **22** | **9 3 1** | **0.88680** | **120.599** | **4.0** |
| **23** | **8 4 4** | **0.86340** | **126.295** | **7.0** |

### II.3.2. UV-Vis Spectrophotometer

Ultraviolet-visible spectroscopy is a spectroscopy technique involving the photons whose wavelengths are in the ultraviolet region (200 nm – 400 nm), visible, and up to the near infrared (750 nm -1400 nm). Subjected to radiation in this range of wavelengths, molecules undergo electronic transitions between ground state and excited states, which causes the absorption of certain lines of radiation incident. This characterization technique provides information on the optical properties of the sample to be analyzed: absorption (A) and reflection (R), transmission (T) of light.

#### II.3.2.1. principle of operation

The basic elements of the spectrophotometer are a light source, the sample, a monochromator to separate the different wavelengths of light, and a detector.

The radiation source is sometimes a tungsten filament (in the $350-1700\ nm$ region), a Deuterium arc lamp which emits a continuous spectrum in the ultraviolet region ($190-400\ nm$), and more recently arc lamps xenon usable throughout the region $UV-Visible$ and light-emitting diodes ($DEL$) for visible wavelengths.

The detector is typically a photodiode, a photomultiplier or a $CCD$ [5].

In a double beam instrument, the light is split into two beams before reaching the sample. One of the beams is used as a reference and crosses a "blank" (same cell and same solvent as the sample), the other passes through the sample.

Samples for the UV-visible spectrophotometer are mostly solutions, although that the absorbance of gauze or solid can also be measured. The samples are supposed in transparent cells, sometimes known as basins. These the cuvettes are characterized as parallelepipedic in shape, with an optical path often of the order 1cm (corresponding to length l in the Beer-Lambert laws). The test tubes can also be used as cuvettes in some instruments. The type of sample container used must allow the passage of the wavelengths of the range of interest. the most used cuvettes are usually made of high quality fused silica or quartz because they are

transparent in the UV-visible and near-infrared regions. Glass and plastic cuvettes are also common, although if glass and most plastic absorb in the UV, which limits their visible and near infrared use [5].

Experimentally, we can obtain the value of Eg usually using the Tauc relation which is given by this equation [6]:

$$(\alpha h\upsilon)^2 = \alpha_0(h\upsilon - E_g) \dots\dots \text{II. 5}$$

Where: $\alpha_0$ is a constant, $E_g$ is the gap energy and $\alpha$ is the absorption coefficient given by:

$$\alpha = 2.303\ A/(d) \dots\dots\dots\dots\dots \text{II. 6}$$

d: is the thickness of the sample (in our case d of the cuvette is 1 cm).

A: is the absorbance

hυ: is the photon energy of or :

$$h\upsilon = \frac{1240}{\lambda} \dots\dots\dots\dots\dots\dots \text{II. 7}$$

We draw a graph of $(\alpha h\upsilon)^2$ with respect to (hυ), we can obtain a straight line. This line intersects the $h\nu$ axis at $(\alpha h\upsilon)^2 = 0$. The values of $Eg$ were estimated from this intercept. For powders and liquids, one optical absorbance spectrum is well suited over others.

### II.3.2.2. Experimental apparatus

As part of our study, we measured the absorbance of our powders, using the Dual Beam : (JaskoV-750) spectrophotometer of range spectrum (190 - 1100), which is existingin the active components and materials laboratory LCAM, Larbi Ben Mhidi Oum El Bouaghi university as shown in **Figure II.8.**

**Figure II.8.** Experimental device of the JaskoV-750 type UV-Vis spectrophotometer, measurement cell and powder cell.

### II.3.3. Fourier Transform Infrared Spectroscopy FTIR

IR absorption spectroscopy is a fast, economical and non-destructive physical method commonly used in structural analysis [7], it is provides information on the bonds between atomic nuclei and their arrangements [8].

#### II.3.3.1. principle of operation

In infrared spectrophotometry, the sample is subjected to incident radiation of an infrared light beam whose frequencies are between 4000 $cm-1$ and 400 $cm-1$, corresponding to the vibrational energy domain of the molecules. When the frequency of this radiation is equal to the resonance frequency of the harmonic oscillator, there is absorption of light energy and amplification of molecular vibrations. This excited state lasts only a fraction of a second. The return to the ground state releases the energy which is absorbed in the form of heat.

The infrared spectrum of a sample is established by examining the transmitted light that indicates the amount of energy absorbed at each wavelength. We can then produce spectra in absorbance or transmittance, and indicate the wavelengths of absorption or frequency. The

position of these absorption bands will depend in particular on the difference electro negativity of atoms and their mass [9].

### II.3.3.2. Experimental apparatus

In our study the FTIR measurements were recorded on a spectrophotometer of type JASCO-4700 existing in the Applied Chemistry and Materials Technology Laboratory (ACMTL), Larbi Ben Mhidi Oum el Bouaghi University as shown in **Figure II.9**. Measurements are in mode transmittance.

**Figure II.9.** JASCO FTIR-4700 Fourier Transform Spectroscopy.

## II.4. Photocatalytic tests

### II.4.1. Polluting model

#### II.4.1.1. Methyl Orange MO

In this work we are interested in methyl orange (Figure II.10). Methyl Orange Dye, is one of the well known and widely used amino acid, used in the paper, printing, textile and pharmaceutical industry and laboratories. It is an anionic dye belongs to the azo dye group [10]. The **Table II.7** summarizes the physical and chemical properties of methyl orange.

**Figure II.10.** Methyl Orange (Mo)

**Table II.7.** Physico-chemical properties of Methyl Orange dye [11, 12].

| Name | Methyl Orange |
|---|---|
| Chemical name | Methyl orange,547-58-0, Orange III, Gold orange, Eniamethyl orange, Helianthine |
| Physical state | powder |
| Color | Orange |
| Formula bully | $C_{14}H_{14}N_3NaO_3S$ |
| Density | 1 |
| Mass molar (g/l) | 327.34 |
| Water solubility (g/l) | 5 g/l (25°C) |
| $\lambda_{max}$ (nm) | Ph basic $\lambda_{max}$ =465 nm<br>Ph acid $\lambda_{max}$ = 505 nm |

| | |
|---|---|
| Structure | 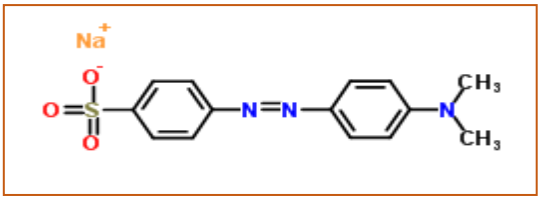 |
| Fusion point | $> 300°C$ |

### II.4.2. Photocatalysts

The catalysts used are nanocomposites based on ZnO and $TiO_2$. They are classified as follows : 20% ZnO/80%$TiO_2$ without calcination and the 80%ZnO/20%$TiO_2$ sample with different calcination temperatures (700,750, 800, 850 and 900°C).

### II.4.3. Type of irradiation used

In this study we use a UV lamp irradiation source. Lamp radiation is electromagnetic radiation composed mainly of ultraviolet (UV) [200-400 nm] and visible (vis) [400-800 nm].

Experimental tests were carried out during the month of May 2023 in five typical days, from 7 may 2023 to 11 May 2023, Chemistry-physics laboratory, Al hadj Lakhdar university of Batna, Algeria.

### II.4.4. Experimental protocol

We followed several steps to carry out the photocatalytic protocol, these steps are as follows:

- First, a stock solution of methyl orange (MO) with a concentration 17 mg/l was prepared.
- Then, 0.5 g of the synthesized nanocomposites are dispersed in 180 ml.
- Next, the suspension of (MO + NCs) obtained is placed in the dark for 40 min to ensure the adsorption and desorption equilibrium with stirring.
- After equilibration (t=0min), the (MO+ NCs) suspension was exposed under a UV lamp with continuous stirring as shown in the **Figure II.11**
- During the irradiation, a quantity of the suspension is taken regularly every 5 minutes until the period of 30 minutes.

- Soon after, the quantities are taken every 10 minutes until the period of 100 minutes.
- Later, the obtained solution is centrifuged to separate the two phases of (MO+NCS).
- Finally, the absorbance of the extracted solution was measured with a UV-Vis absorption spectrophotometer in the range 465 nm.

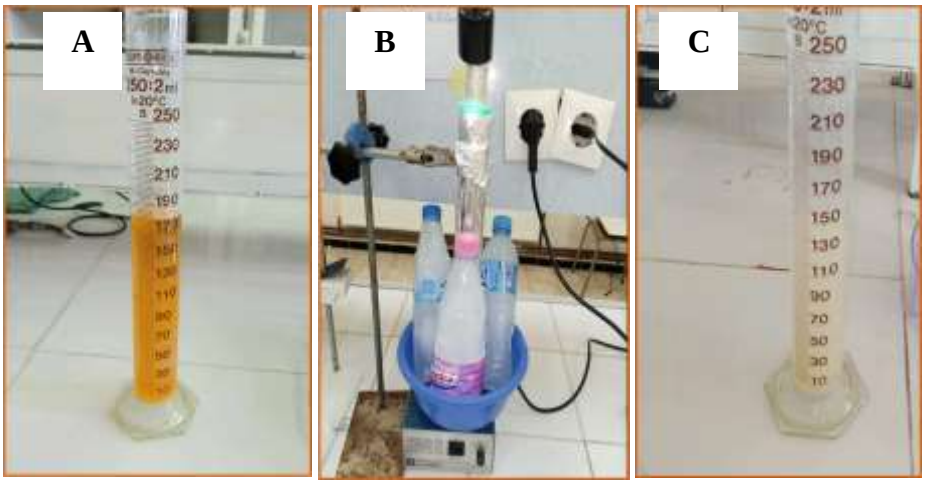


**Figure II.11.** (MO+ NCs) suspension: A) Before irradiation, B) During irradiation, C) After irradiation

## II.4. Conclusion

In this chapter, we have presented, the synthesis of nanocomposites based of ZnO and $TiO_2$ by the Sol- gel method. Then we presented the equipment and techniques used to characterize the prepared samples. Finally we described the experimental procedure regarding the use of these nanocomposites as catalysts to degrade methyl orange (MO) under UV irradiation.

## References

[1] A. Mebrek, Elaboration et caractérisation de céramiques ZnO-$TiO_2$, thèse de doctorat, Université Badji Mokhtar –Annaba, Algérie, (2018), p 34.

[2] A. Gaddari, Nouvelle méthode d'élaboration par voie sol-gel des couches minces de dioxyde d'étain : Applications à la détection à température ambiante d'ozone et d'ammoniac, thèse de Doctorat, Université de Franche-Comté, France, (2013), p 60.

[3] S. Rahmane, Elaboration et Caractérisation de couches minces par spray pyrolyse et pulvérisation magnétron, thèse doctorat, Université Mohamed Kheider-Biskra, Algérie, (2008), p 29.

[4] M. Dahnoun, Preparation and characterization of Titanium dioxide and Zinc oxide thin films via Sol-Gel (spin coating) technique for optoelectronic applications, doctoral thesis, University Mohamed Kheider of Biskra, Algeria, (2020), p 31.

[5] R. Messadia, Elaboration et caractérisation des nanoparticules de ZnO par co-précipitation, Application à la photo dégradation de méthyle orange, mémoire master, Université Badji Mokhtar Annaba, Algérie, (2018), p 24-25-26.

[6] J. Tauc, Optical properties and electronic structure of amorphous Ge and Si, Materials Research Bulletin, 3 (1968) p 37-46.

[7] F. Gomri, étude des interfaces solide-liquide: Application à l'adsorption des micropolluants, thèse de doctorat Université Ferhat Abbas setif 1, Algérie, (2017), p 48.

[8] M. L. Ettorche, Etude des propriétés structurales de matériaux semiconducteurs finement cristallisés incorporés dans des matrices hôtes, thèse doctorat, Université Constantine 1, Algérie, ( 2014), p 23.

[9] S.E. Abdoun, R. Achiche, Synthèse de nanocomposites à base de ZnO par la méthode hydrothermale et leurs applications à photodegradation photocatalytique et antibactérienne, mémoire master, Université Larbi Ben Mhidi Oum El Bouaghi, Algérie, (2021), p 53.

[10] M. Tir, S. Kadri, Elimination du colorant (Méthyl orange) par les hydroxydes doubles lamellaires (HDLs), mémoire master, Université de Echahid Hamma Lakhdar- El-Oued, Algérie, (2018), p 15.

[11] S. O. Mohamed, A. Bacha, Adsorption des colorants « orange de méthyle » par charbon actif, mémoire master, Université el- wancharissi de tissemsilt, Algérie, (2018), p 51.

[12] L. Belouettar, Etude de décoloration du méthyle orange en milieu hétérogène, mémoire master, Université de Badji Mokhtar –Annaba, Algérie, (2020), p 19.

# Chapter III

# Results and Interpretations

## III.1. Introduction

In this chapter we present the results obtained from the preparation of the ZnO and $TiO_2$ nanocomposites by sol-gel method. We study (i) the effect of different percent of ZnO and $TiO_2$ in the (ZnO and $TiO_2$) nanocomposites on the structural and optical properties, (ii) the effect of calcination temperatures in the ZnO and $TiO_2$ nanocomposites prepared with (80% ZnO and 20% $TiO_2$) on the structural and optical properties. In addition to this, we focus on enhancing photocatalytic activity by modifying percent of (ZnO and $TiO_2$) and calcination temperatures in the prepared nanocomposites.

## III.1. Effect of different percent of ZnO and $TiO_2$ in (ZnO and $TiO_2$) nanocomposites on the structural and optical properties

### III.1.1. Structural Properties

**Figure III.1** shows the X-ray diffraction spectra of (ZnO and $TiO_2$) nanocomposites prepared with different percentages of (ZnO and $TiO_2$) which are ;

(65% ZnO/35% $TiO_2$ ,75% ZnO/25% $TiO_2$ ,80% ZnO/20% $TiO_2$ ,85% ZnO/15% $TiO_2$)

The peaks observed at 2θ =32.182°, 34.878°, 36.545°, 47.729°, 62.803° and 68.439° marked by their miller indices (100) ,(002) ,(101) ,(102) ,(103) and (112) corresponded to hexagonal phase of ZnO (JCPDS card no 36-1451) in addition the peaks marked at 2θ =56.60° and 74.89° considerable by their miller indices (511) and (622) , obvious to cubic phase of $Zn_2TiO_4$ (JCPDS card no 25-1164).

We note that, the increase in the percentages of ZnO (decrease in the percentages of $TiO_2$) leads to the improvement of the crystallinity, since the intensities of the peaks become more intense.

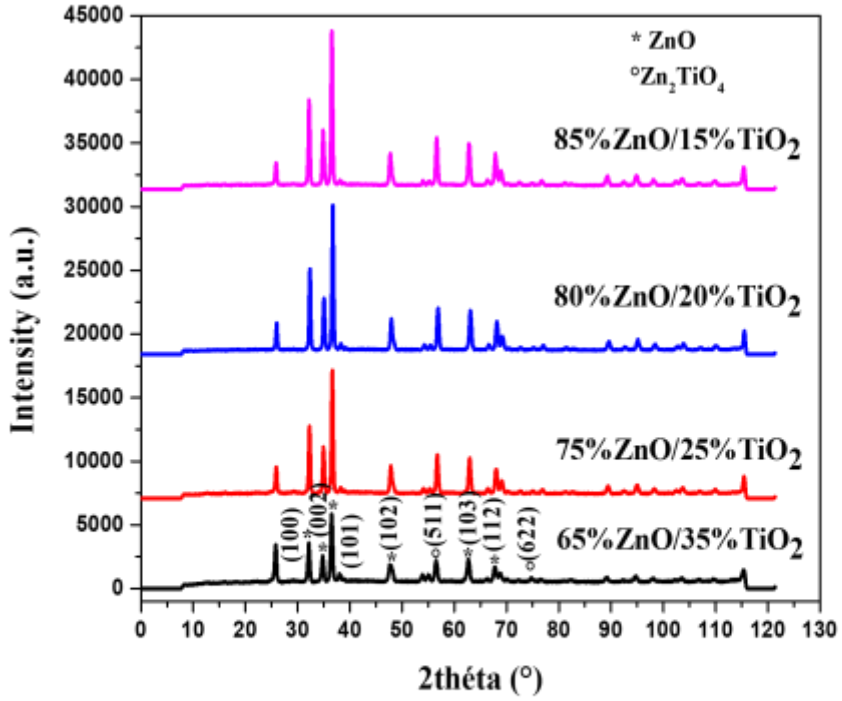


**Figure III.1.** *X*RD spectra of ($ZnO/TiO_2$) nanocomposites prepared with different percentages of (ZnO and $TiO_2$)

❖ **Estimation of lattice parameters (a, c) and crystallite size:**

The information concerning the diffraction peaks such as the position (2θ), intensity (I) and full width at half maximum (FWHM) are summarized in **Table III.1**. To find the interlattice distance $d_{hkl}$ we used Bragg's law (Formula III.1). However, to find the lattice parameters we use the formulas (III. 3 and 4), and finally to estimate the size of the crystallites we use the Debye–Scherrer law (formula III.5).

➢ **The inter-reticular distance d (hkl)**

According to Bragg's law: $2d_{hkl}\sin\theta = n\lambda$ ……. III. 1

$$\longrightarrow \quad d_{hkl} = \frac{\lambda}{2\sin\theta}\,(A°)\ldots\ldots\text{III.2}$$

Knowing that the wavelength $\lambda = 1.5406 A°$

- **Mesh parameters (a, c)**

Mesh parameters of the hexagonal structure is given by these formulas:

$$a = \sqrt{\frac{\lambda^2(h^2 + k^2 + l^2)}{4\sin^2\theta}} \dots\dots \text{III. 3}$$

$$C = \frac{\lambda}{\sin\theta} \dots\dots\dots \text{III. 4}$$

Mesh parameters of the cubic structure is given by this formula:

$$a = \frac{n\lambda\sqrt{h^2+k^2+l^2}}{2\sin\theta} \text{.....III.5}$$

In cubic structure mesh parameters a and c are equal a=c, as shown in the following **Figure III.2.**

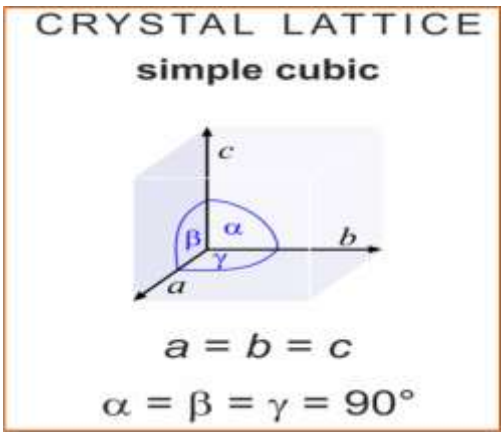


**Figure III.2.** Single cubic lattice [1].

- **The average crystallite size *Dmoy***

To estimate the crystallite sizes the Debye–Scherrer law is used

$$D = \frac{k\lambda}{\beta\cos\theta_\beta} \text{.....III.6}$$

$$D = \frac{0.9 \times 0.15406}{\text{FWHM(rad)} \times \cos\frac{2\theta}{2}} \text{ (nm)} \dots\dots\dots\dots\dots \text{III. 7}$$

Knowing that the wavelength $\lambda = 1.5406 A°$

From **Figure III.3** showing the Gaussian adjustment method of diffraction peaks we determined the "full width at half maximum" values of different peaks.

- **The mesh volume V**

The volume of the hexagonal structure is given by using the formula (III.8) [2]:

$$V = \frac{\sqrt{3}}{2} a^2 c \ldots\ldots\ldots\ldots\ldots\ldots\ldots\ldots\ldots\ldots \text{III. 8}$$

The volume of the cubic structure is given by the formula (III.9) [3]:

$$V = a^3 \ldots\ldots\ldots\ldots\ldots\ldots \text{III. 9}$$

The lattice strain and dislocation density are estimated using the formulas (III.10 and 11) [4,2]:

- **lattice strain ε**

$$\varepsilon = \frac{FWHM}{4 \times \tan\left(\frac{2\theta}{2}\right)} \ldots\ldots\ldots\ldots\ldots \text{III. 10}$$

- **dislocation density δ**

$$\delta = \frac{1}{D^2} \ldots\ldots\ldots \text{III. 11}$$

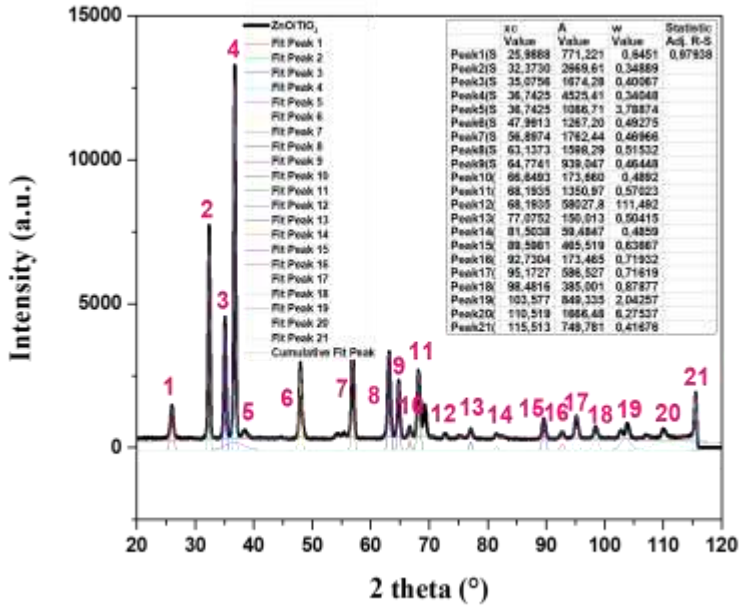


**Figure III.3.** Gaussian adjustment method of diffraction peaks, ($Xc$ = 2θ ; = $Int$and$W$ = $FWHM$).

**Table III.1.** Structural parameters lattice parameters (a, c ) , "full width at half maximum" values (FWHM, β) and inter –planar spacing (d)

Where the numbers 1,2,3,4 represents the percents: 65% ZnO/35% $TiO_2$, 75% ZnO/25% $TiO_2$, 80% ZnO/20% $TiO_2$, 85% ZnO/15% $TiO_2$ respectively.

| N° | samples | phases | 2θ (°) | (hkl) plan | Intensity (a.u.) | FWHM (°) | a (nm) | c (nm) | d (nm) |
|---|---|---|---|---|---|---|---|---|---|
| 1 | ZnO/$TiO_2$ | ZnO Wurtzite | 32,267 | (100) | 1968,286 | 0,361 | 0,277 | 0,554 | 0,277 |
| | | | 34,952 | (002) | 1479,999 | 0,409 | 0,513 | 0,513 | 0,256 |
| | | | 36,638 | (101) | 3638,751 | 0,365 | 0,346 | 0,490 | 0,245 |
| | | $Zn_2TiO_4$ | 56,736 | (511) | 1356,691 | 0,454 | 0,842 | 0,842 | 0,161 |
| 2 | ZnO/$TiO_2$ | ZnO Wurtzite | 32,267 | (100) | 1968,286 | 0,361 | 0,277 | 0,554 | 0,277 |
| | | | 34,952 | (002) | 1479,999 | 0,409 | 0,513 | 0,513 | 0,256 |
| | | | 36,638 | (101) | 3638,751 | 0,365 | 0,346 | 0,490 | 0,245 |
| | | $Zn_2TiO_4$ | 56,736 | (511) | 1356,691 | 0,454 | 0,842 | 0,842 | 0,161 |
| 3 | ZnO/$TiO_2$ | ZnO Wurtzite | 32,267 | (100) | 1968,286 | 0,361 | 0,277 | 0,554 | 0,277 |
| | | | 34,952 | (002) | 1479,999 | 0,409 | 0,513 | 0,513 | 0,256 |
| | | | 36,638 | (101) | 3638,751 | 0,365 | 0,346 | 0,490 | 0,245 |
| | | $Zn_2TiO_4$ | 56,736 | (511) | 1356,691 | 0,454 | 0,842 | 0,842 | 0,161 |
| 4 | ZnO/$TiO_2$ | ZnO Wurtzite | 32,267 | (100) | 1968,286 | 0,361 | 0,277 | 0,554 | 0,277 |
| | | | 34,952 | (002) | 1479,999 | 0,409 | 0,513 | 0,513 | 0,256 |
| | | | 36,638 | (101) | 3638,751 | 0,365 | 0,346 | 0,490 | 0,245 |
| | | $Zn_2TiO_4$ | 56,736 | (511) | 1356,691 | 0,454 | 0,842 | 0,842 | 0,161 |

**Table III.1** shows structural parameters lattice parameters (a, c), value of the full width at half maximum (FWHM, β) ,inter –planar spacing (d) obtained by the analysis of the XRD spectra;

We notice that a, c and d values are in agreement with the JCPDS data files [00-036-1451] and [00-025-1164]. Also a, c and d values are consistent with published work [2].

**Table III.2.** Structural parameters crystallite size (D), average crystallite size ($D_{moy}$), cell volume (V), dislocation density (δ) and lattice strain (ε) estimated by the analysis of XRD spectra.

| N° | samples | phases | 2θ (°) | (hkl) plan | D (nm) | $D_{moy}$ (nm) | V (A°) | δ (nm) | ε ($10^{-3}$) |
|---|---|---|---|---|---|---|---|---|---|
| 1 | ZnO/$TiO_2$ | ZnO Wurtzite | 32,267 | (100) | 22,883 | 22,040 | 36,812 | 0,0019 | 0,456 |
| | | | 34,952 | (002) | 20,347 | | 116,918 | 0,0024 | 0,562 |
| | | | 36,638 | (101) | 22,890 | | 50,801 | 0,0019 | 0,528 |

| | | | | | | | | | |
|---|---|---|---|---|---|---|---|---|---|
| | | $Zn_2TiO_4$ | 56,736 | (511) | 19,844 | - | 569,947 | 0,0025 | 1,072 |
| 2 | $ZnO/TiO_2$ | ZnO Wurtzite | 32,267 | (100) | 22,883 | 22,040 | 36,812 | 0,0019 | 0,456 |
| | | | 34,952 | (002) | 20,347 | | 116,918 | 0,0024 | 0,562 |
| | | | 36,638 | (101) | 22,890 | | 50,801 | 0,0019 | 0,528 |
| | | $Zn_2TiO_4$ | 56,736 | (511) | 19,844 | - | 569,947 | 0,0025 | 1,072 |
| 3 | $ZnO/TiO_2$ | ZnO Wurtzite | 32,267 | (100) | 22,883 | 22,040 | 36,812 | 0,0019 | 0,456 |
| | | | 34,952 | (002) | 20,347 | | 116,918 | 0,0024 | 0,562 |
| | | | 36,638 | (101) | 22,890 | | 50,801 | 0,0019 | 0,528 |
| | | $Zn_2TiO_4$ | 56,736 | (511) | 19,844 | - | 569,947 | 0,0025 | 1,072 |
| 4 | $ZnO/TiO_2$ | ZnO Wurtzite | 32,267 | (100) | 22,883 | 22,040 | 36,812 | 0,0019 | 0,456 |
| | | | 34,952 | (002) | 20,347 | | 116,918 | 0,0024 | 0,562 |
| | | | 36,638 | (101) | 22,890 | | 50,801 | 0,0019 | 0,528 |
| | | $Zn_2TiO_4$ | 56,736 | (511) | 19,844 | | 569,947 | 0,0025 | 1,072 |

**Table III.2** shows structural parameters; crystallite size (D) ,average crystallite size ($D_{moy}$) ,cell volume (V) ,dislocation density (δ) , lattice strain (ε) estimated by the analysis of the spectra of XRD ,

We observe that the values of cell volume (V), dislocation density (δ) and lattice strain (ε) are in agreement with those published in previous studies [2]. The average crystallite size in the hexagonal phase of ZnO and the crystallite size in the $Zn_2TiO_4$ phase are not changed with the percentages of ZnO and $TiO_2$, their values are 22,040 nm and 19.844 nm, respectively. This indicates that the percentages of ZnO and $TiO_2$ do not alter the crystallite sizes of the existing phases.

### III.1.2. optical Properties

#### III.1.2.1. Optical gap

**FigureIII.4** shows the UV-Visible absorbance spectra of ZnO and $TiO_2$ based nanocomposites prepared with different percentages of ZnO and $TiO_2$ which are (65% ZnO/35% $TiO_2$, 75% ZnO/25% $TiO_2$, 80% ZnO/20% $TiO_2$, 85% ZnO/15% $TiO_2$)

As we can seen, for all samples there is (i) a clear absorption edge in the wavelength range of UV [200 nm- 400nm] (ii) significant absorbance around 0.8 in the ultra violet range (200-400nm) which allows this nanocomposite to be used in important applications such as protection against solar radiation.

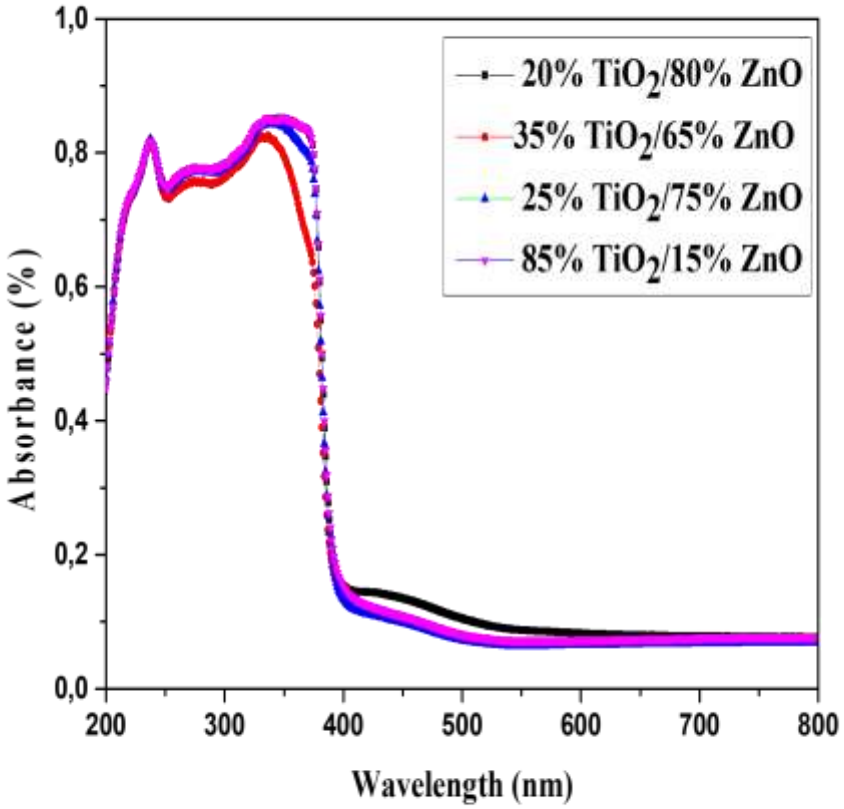


**Figure III.4.** UV-Visible absorbance spectra of ZnO and $TiO_2$ based nanocomposites prepared with different percentages of (ZnO and $TiO_2$) which are (65% ZnO/35% $TiO_2$ ,75% ZnO/25% $TiO_2$ ,80% ZnO/20% $TiO_2$ ,85% ZnO/15% $TiO_2$).

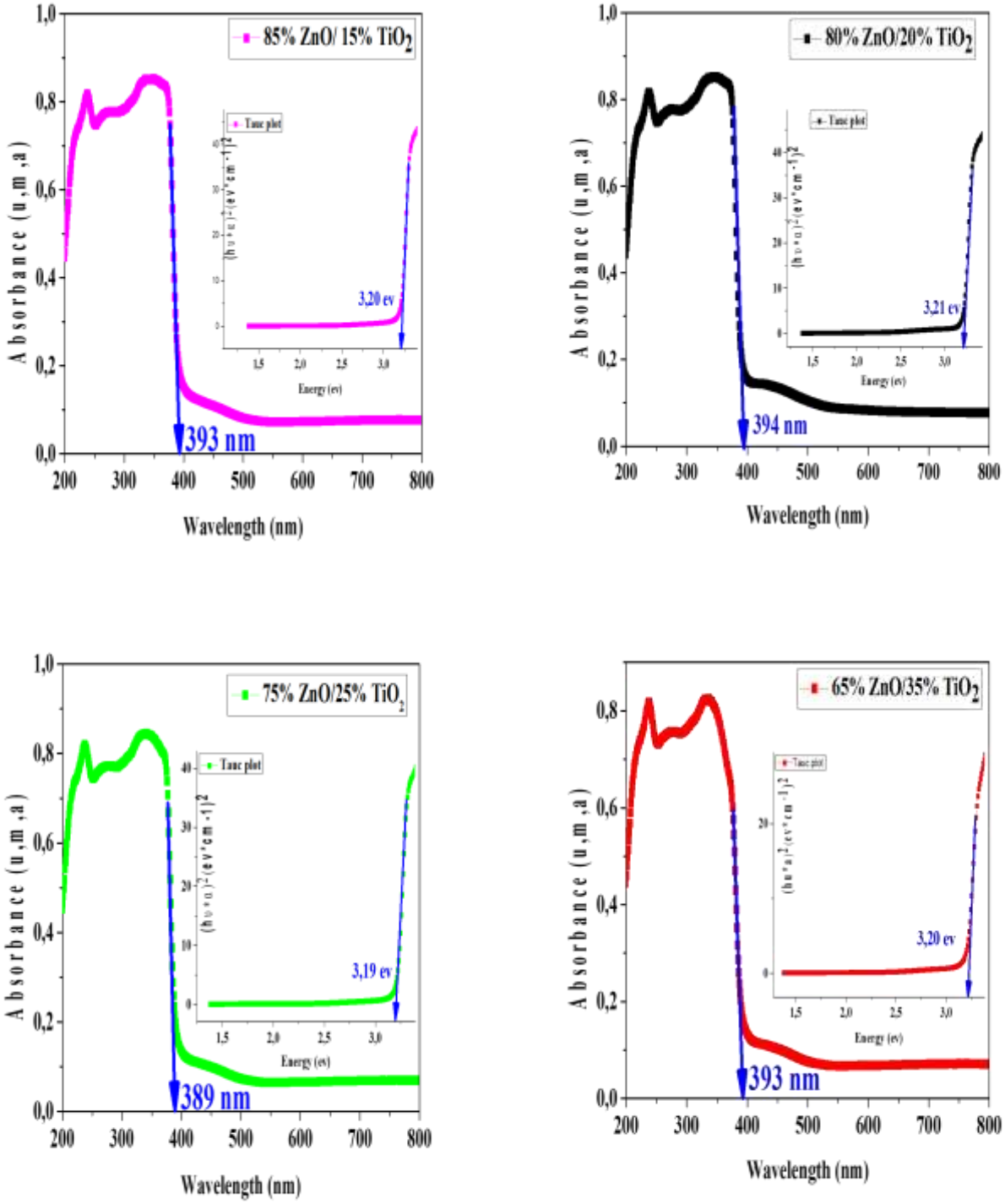


**Figure III.5.** Spectral dependence of (αhυ) and photon energy (hυ), used to estimate the band gab value Eg of 80% ZnO/20% $TiO_2$, 65%ZnO/35%$TiO_2$, 75%ZnO/25%$TiO_2$ and 85%ZnO/15%$TiO_2$ samples

### III.1.2.2. Estimation of the band Gab energy

**Figure III.5 shows** Spectral dependence of (αhυ) and photon energy (hυ), used to estimate the band gab value Eg of the prepared samples.

The band gab energy Eg is obtained from the interception of the linear portion of $(\alpha h\upsilon)^2$ vs (hυ), using Tauc method (Eq III.12). The Tauc curves have been shown in **Figure III.5.**

$$(\alpha h\upsilon)^2 = A(h\upsilon - Eg) \ldots\ldots\ldots\ldots \text{III.12}$$

Where A is a constant, hυ is the photon energy, and Eg is the band energy gap, α is the absorption coefficient :

$$\alpha = 2.303 \times A \ldots\ldots\ldots\ldots\ldots\ldots \text{III. 13}$$

$$h\upsilon = \frac{1240}{\lambda} \ldots\ldots\ldots\ldots\ldots\ldots\ldots\ldots \text{III. 14}$$

In **Figure III.6** show the variation of $(\alpha h\upsilon)^2$ vas function of (hυ) for all samples,

The absorption edge in the (85% ZnO/15% $TiO_2$) sample is equal to 393 nm, the gap estimate gives 3.20 eV.

The absorption edge in the (80% ZnO/20% $TiO_2$) sample is equal to 394 nm, the gap estimate gives 3.21 eV.

The absorption edge in the (75% ZnO/25% $TiO_2$) sample is equal to 389nm , the gap estimate gives 3.19 eV.

The absorption edge in the (65% ZnO/35% $TiO_2$) sample is equal to 387 nm , the gap estimate gives 3.20 eV.

**Figure III.6** shows the variation of the obtained optical gap of ZnO and $TiO_2$ nanocomposites as function of percentages. The values of the optical gaps obtained for (85% ZnO/15% $TiO_2$) ,(80% ZnO/20% $TiO_2$) ,(75% ZnO/25% $TiO_2$) ,(65% ZnO/35% $TiO_2$) are 3.20, 3.21, 3.19 and 3.20 respectively, which are consistent with the values found in the literature [2,5].



The gap value increases for the sample (75% ZnO/25% $TiO_2$) until reaching 3.21 eV then decreases to 3.19 eV for the sample (80% ZnO/20% $TiO_2$).

## III.2.Effect of calcination temperature on the structural and optical properties

### III.2.1.structural properties

**Figure III.7** shows the X-ray diffraction spectra of (80%ZnO/20%$TiO_2$) nanocomposites calcined in different temperatures (300 °C, 700°C, 750°C, 800°C, 850°C and 900°C).

The peaks remarked at 2θ =32.25°, 47.81° ,56.65° ,62.97° ,69.12° and 115,532 noticeable by their miller indices (100) ,(102) ,(110) ,(103) ,(201) and (213), proportionate to hexagonal phase of ZnO (JCPDS card no. 36-1451 ) in addition the peaks perceived at 2θ= 35.58° ,36.54° and 64.76°, relative by their miller indices (311) ,(222) and (531) matching to cubic phase of $Zn_2TiO_4$ (JCPDS card no.25-1164) .

After calcination in (700°C,750°C ,800°C ,850°C ,900°C) , we distinguish the emergence of weak peaks, this is explained by the possibility of the presence of impurities that were previously present in the dig (creuset).

We mention that the peaks located at 2θ=64,76° and 35,58° corresponding to the (531) and (311) plans do not appear when the calcination temperature increases above 300°C.

We note that there is a difference between the sample calcined in the temperature 300°C and the other samples calcined at the temperatures 700, 750, 800, 850 and 900°C. Hence the diffraction spectra of the calcined samples in temperatures above 300°C show the emergence of peaks located at 2θ=30.63°, 43.26° and 53.38° corresponding to planes 220),( 400) ,(422) of the $Zn_2TiO_4$ phase

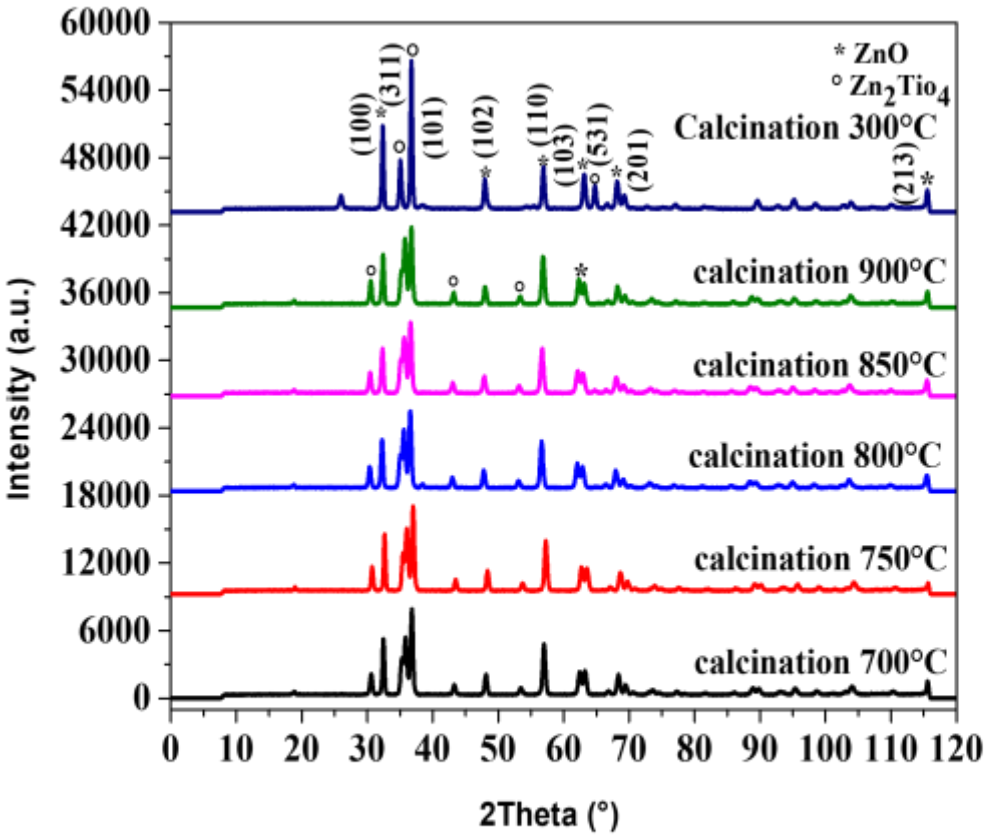


**Figure III.7.** *X*RD spectra of 80% ZnO/ 20% $TiO_2$nanocomposites calcined in different calcination temperatures (300°C, 700°C,750°C,800°C,850°C and 900°C).

**Table III.3.** Structural parameters; (a, c ) lattice parameters , value of the full width at half maximum (FWHM, β), inter –planar spacing (d).
attained by the analysis of the XRD spectra.

| N° | samples | phases | 2θ (°) | (hkl) plan | Intensity (a.u.) | FWHM (°) | a (nm) | c (nm) | d (nm) |
|---|---|---|---|---|---|---|---|---|---|
| 300° | $ZnO/TiO_2$ | ZnO Wurtzite | 32,373 | (100) | 2652,123 | 0,004 | 0,276 | 0,552 | 0,276 |
| | | | 47,992 | (102) | 1329,020 | 0,510 | 0,423 | 0,378 | 0,189 |
| | | | 56,897 | (110) | 1843,325 | 0,484 | 0,228 | 0,323 | 0,161 |
| | | $Zn_2TiO_4$ | 35,075 | (311) | 1671,927 | 0,400 | 0,847 | 0,847 | 0,255 |
| | | | 36,742 | (222) | 4527,228 | 0,340 | 0,846 | 0,846 | 0,244 |
| 700° | $ZnO/TiO_2$ | ZnO Wurtzite | 32,474 | (100) | 1908,115 | 0,369 | 0,275 | 0,550 | 0,275 |
| | | | 48,125 | (102) | 853,859 | 0,458 | 0,422 | 0,377 | 0,188 |
| | | | 57,000 | (110) | 2351,470 | 0,512 | 0,228 | 0,322 | 0,161 |
| | | $Zn_2TiO_4$ | 18,852 | (111) | 108,444 | 0,464 | 0,814 | 0,814 | 0,470 |
| | | | 30,602 | (220) | 835,324 | 0,441 | 0,825 | 0,852 | 0,291 |
| | | | 35,724 | (311) | 4732,909 | 1,043 | 0,832 | 0,832 | 0,251 |
| | | | 36,817 | (222) | 3193,978 | 0,414 | 0,844 | 0,844 | 0,243 |
| 750° | $ZnO/TiO_2$ | ZnO Wurtzite | 32,474 | (100) | 1908,115 | 0,369 | 0,275 | 0,550 | 0,275 |
| | | | 48,125 | (102) | 853,859 | 0,458 | 0,422 | 0,377 | 0,188 |
| | | | 57,000 | (110) | 2351,470 | 0,512 | 0,228 | 0,322 | 0,161 |
| | | $Zn_2TiO_4$ | 18,852 | (111) | 108,444 | 0,464 | 0,814 | 0,814 | 0,470 |
| | | | 30,602 | (220) | 835,324 | 0,441 | 0,825 | 0,852 | 0,291 |
| | | | 35,724 | (311) | 4732,909 | 1,043 | 0,832 | 0,832 | 0,251 |
| | | | 36,817 | (222) | 3193,978 | 0,414 | 0,844 | 0,844 | 0,243 |
| 800° | $ZnO/TiO_2$ | ZnO Wurtzite | 32,474 | (100) | 1908,115 | 0,369 | 0,275 | 0,550 | 0,275 |
| | | | 48,125 | (102) | 853,859 | 0,458 | 0,422 | 0,377 | 0,188 |
| | | | 57,000 | (110) | 2351,470 | 0,512 | 0,228 | 0,322 | 0,161 |
| | | $Zn_2TiO_4$ | 18,852 | (111) | 108,444 | 0,464 | 0,814 | 0,814 | 0,470 |
| | | | 30,602 | (220) | 835,324 | 0,441 | 0,825 | 0,852 | 0,291 |
| | | | 35,724 | (311) | 4732,909 | 1,043 | 0,832 | 0,832 | 0,251 |
| | | | 36,817 | (222) | 3193,978 | 0,414 | 0,844 | 0,844 | 0,243 |
| 850° | $ZnO/TiO_2$ | ZnO Wurtzite | 32,474 | (100) | 1908,115 | 0,369 | 0,275 | 0,550 | 0,275 |
| | | | 48,125 | (102) | 853,859 | 0,458 | 0,422 | 0,377 | 0,188 |
| | | | 57,000 | (110) | 2351,470 | 0,512 | 0,228 | 0,322 | 0,161 |
| | | $Zn_2TiO_4$ | 18,852 | (111) | 108,444 | 0,464 | 0,814 | 0,814 | 0,470 |
| | | | 30,602 | (220) | 835,324 | 0,441 | 0,825 | 0,852 | 0,291 |
| | | | 35,724 | (311) | 4732,909 | 1,043 | 0,832 | 0,832 | 0,251 |
| | | | 36,817 | (222) | 3193,978 | 0,414 | 0,844 | 0,844 | 0,243 |
| 900° | $ZnO/TiO_2$ | ZnO Wurtzite | 32,474 | (100) | 1908,115 | 0,369 | 0,275 | 0,550 | 0,275 |
| | | | 48,125 | (102) | 853,859 | 0,458 | 0,422 | 0,377 | 0,188 |
| | | | 57,000 | (110) | 2351,470 | 0,512 | 0,228 | 0,322 | 0,161 |
| | | $Zn_2TiO_4$ | 18,852 | (111) | 108,444 | 0,464 | 0,814 | 0,814 | 0,470 |
| | | | 30,602 | (220) | 835,324 | 0,441 | 0,825 | 0,852 | 0,291 |
| | | | 35,724 | (311) | 4732,909 | 1,043 | 0,832 | 0,832 | 0,251 |
| | | | 36,817 | (222) | 3193,978 | 0,414 | 0,844 | 0,844 | 0,243 |

**Table III.3** shows structural parameters earned by the analysis of the spectra XRD: we notice that a, c and d values are in agreement with the JCPDS data files [00-036-1451] and [00-025-1164]. Also a, c and d values are consistent with published work [2]

**Table III.4.** Structural parameters crystallite size (D), average crystallite size ($D_{moy}$), cell volume (V), dislocation density (δ) and lattice strain (ε) estimated by the analysis of XRD spectra.

| N° | samples | phases | 2θ (°) | (hkl) plan | D (nm) | $D_{moy}$ (nm) | V (A°) | δ (nm) | ε ($10^{-3}$) |
|---|---|---|---|---|---|---|---|---|---|
| 300° | $ZnO/TiO_2$ | ZnO Wurtzite | 32,373 | (100) | 2068,051 | 701,256 | 36,415 | $2,3.10^{-7}$ | 0,005 |
| | | | 47,992 | (102) | 17,050 | | 58,573 | 0,0034 | 0,990 |
| | | | 56,897 | (110) | 18,668 | | 14,541 | 0,0028 | 1,144 |
| | | $Zn_2TiO_4$ | 35,075 | (311) | 20,828 | 22,724 | 607,645 | 0,0023 | 0,551 |
| | | | 36,742 | (222) | 24,620 | | 605,495 | 0,0016 | 0,492 |
| 700° | $ZnO/TiO_2$ | ZnO Wurtzite | 32,474 | (100) | 22,423 | 19,691 | 36,021 | 0,0019 | 0,468 |
| | | | 48,125 | (102) | 18,996 | | 58,142 | 0,0027 | 0,892 |
| | | | 57,000 | (110) | 17,655 | | 14,490 | 0,0032 | 1,213 |
| | | $Zn_2TiO_4$ | 18,852 | (111) | 17,355 | 16,064 | 539,353 | 0,0033 | 0,336 |
| | | | 30,602 | (220) | 18,676 | | 561,515 | 0,0028 | 0,526 |
| | | | 35,724 | (311) | 8,002 | | 575,930 | 0,015 | 1,466 |
| | | | 36,817 | (222) | 20,223 | | 601,211 | 0,0024 | 0,601 |
| 750° | $ZnO/TiO_2$ | ZnO Wurtzite | 32,474 | (100) | 22,423 | 19,691 | 36,021 | 0,0019 | 0,468 |
| | | | 48,125 | (102) | 18,996 | | 58,142 | 0,0027 | 0,892 |
| | | | 57,000 | (110) | 17,655 | | 14,490 | 0,0032 | 1,213 |
| | | $Zn_2TiO_4$ | 18,852 | (111) | 17,355 | 16,064 | 539,353 | 0,0033 | 0,336 |
| | | | 30,602 | (220) | 18,676 | | 561,515 | 0,0028 | 0,526 |
| | | | 35,724 | (311) | 8,002 | | 575,930 | 0,015 | 1,466 |
| | | | 36,817 | (222) | 20,223 | | 601,211 | 0,0024 | 0,601 |
| 800° | $ZnO/TiO_2$ | ZnO Wurtzite | 32,474 | (100) | 22,423 | 19,691 | 36,021 | 0,0019 | 0,468 |
| | | | 48,125 | (102) | 18,996 | | 58,142 | 0,0027 | 0,892 |
| | | | 57,000 | (110) | 17,655 | | 14,490 | 0,0032 | 1,213 |
| | | $Zn_2TiO_4$ | 18,852 | (111) | 17,355 | 16,064 | 539,353 | 0,0033 | 0,336 |
| | | | 30,602 | (220) | 18,676 | | 561,515 | 0,0028 | 0,526 |
| | | | 35,724 | (311) | 8,002 | | 575,930 | 0,015 | 1,466 |
| | | | 36,817 | (222) | 20,223 | | 601,211 | 0,0024 | 0,601 |
| 850° | $ZnO/TiO_2$ | ZnO Wurtzite | 32,474 | (100) | 22,423 | 19,691 | 36,021 | 0,0019 | 0,468 |
| | | | 48,125 | (102) | 18,996 | | 58,142 | 0,0027 | 0,892 |
| | | | 57,000 | (110) | 17,655 | | 14,490 | 0,0032 | 1,213 |
| | | $Zn_2TiO_4$ | 18,852 | (111) | 17,355 | 16,064 | 539,353 | 0,0033 | 0,336 |
| | | | 30,602 | (220) | 18,676 | | 561,515 | 0,0028 | 0,526 |
| | | | 35,724 | (311) | 8,002 | | 575,930 | 0,015 | 1,466 |
| | | | 36,817 | (222) | 20,223 | | 601,211 | 0,0024 | 0,601 |
| 900° | $ZnO/TiO_2$ | ZnO Wurtzite | 32,474 | (100) | 22,423 | 19,691 | 36,021 | 0,0019 | 0,468 |
| | | | 48,125 | (102) | 18,996 | | 58,142 | 0,0027 | 0,892 |

| | | | | | | | | | |
|---|---|---|---|---|---|---|---|---|---|
| | | | **57,000** | **(110)** | **17,655** | | **14,490** | **0,0032** | **1,213** |
| | | **$Zn_2TiO_4$** | **18,852** | **(111)** | **17,355** | **16,064** | **539,353** | **0,0033** | **0,336** |
| | | | **30,602** | **(220)** | **18,676** | | **561,515** | **0,0028** | **0,526** |
| | | | **35,724** | **(311)** | **8,002** | | **575,930** | **0,015** | **1,466** |
| | | | **36,817** | **(222)** | **20,223** | | **601,211** | **0,0024** | **0,601** |

**Table III.4** shows structural parameters ; crystallite size (D), average crystallite size ($D_{moy}$) , cell volume (V) , dislocation density (δ) and lattice strain (ε) achieved by the analysis of the spectra of XRD.

We observe that the values of cell volume (V), dislocation density (δ) and lattice strain (ε) are in agreement with those published in previous studies [2]. For the different samples prepared, the average crystallite size in the ZnO hexagonal phase is equal to 19.691 nm for all the samples. Also, the average crystallite size in the $Zn_2TiO_4$ phase does not change with the calcinations temperatures (700-900°C), it is equal to 16.064 nm. We mention that the average crystallite size, in the hexagonal phase of ZnO and in the $Zn_2TiO_4$ phase do not vary with calcination temperatures (700-900°C) in the (80%ZnO/20%$TiO_2$) nanocomposites, this indicates that the latter does not alter the crystallite size in the existing phases. We note that in the sample calcined in 300°C the average crystallite size in the ZnO hexagonal phase and the $Zn_2TiO_4$ phase are equal to 701.25 nm and 22.72 nm, respectively.

This indicates that the average crystallite size decreases when the calcination temperature increases.

### III.3.2.optical properties

#### III.3.2.1. Optical gap

**FigureIII.8** shows the UV-Visible absorbance spectra of (80% ZnO and 20%$TiO_2$) based nanocomposites prepared in different calcinations temperatures (300,700, 750,800, 850, 900°C)

As we can seen, for all samples there is (i) a clear absorption edge in the wavelength range of UV [200 nm- 400nm] (ii) significant absorbance around 0.8 in the ultra violet range (200-400nm) which allows this nanocomposite to be used in important applications such as protection against solar radiation.

The absorbance of the samples in the wavelength range between 200 nm and 400 nm, it varies between 0.85 and 0.71 for all the samples, which means that the calcination temperature has an influence on the absorbance. The sample calcined in 300 and 900°C have

relatively the highest absorbances (≈ 0.85) while the lowest absorbance is recorded in the sample calcined in 700°C (≈ 0.71).

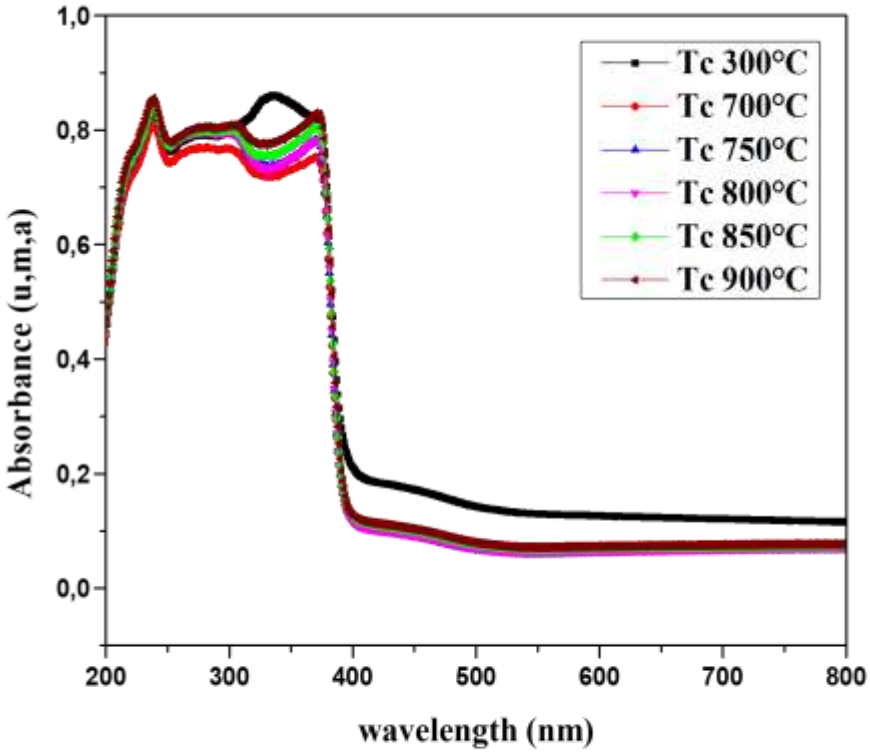


**Figure III.8.** UV-Visible absorbance spectra of 80% ZnO/ 20% $TiO_2$nanocomposites in different calcination temperatures (300°C,700°C,750°C,800°C,850°C,900°C).

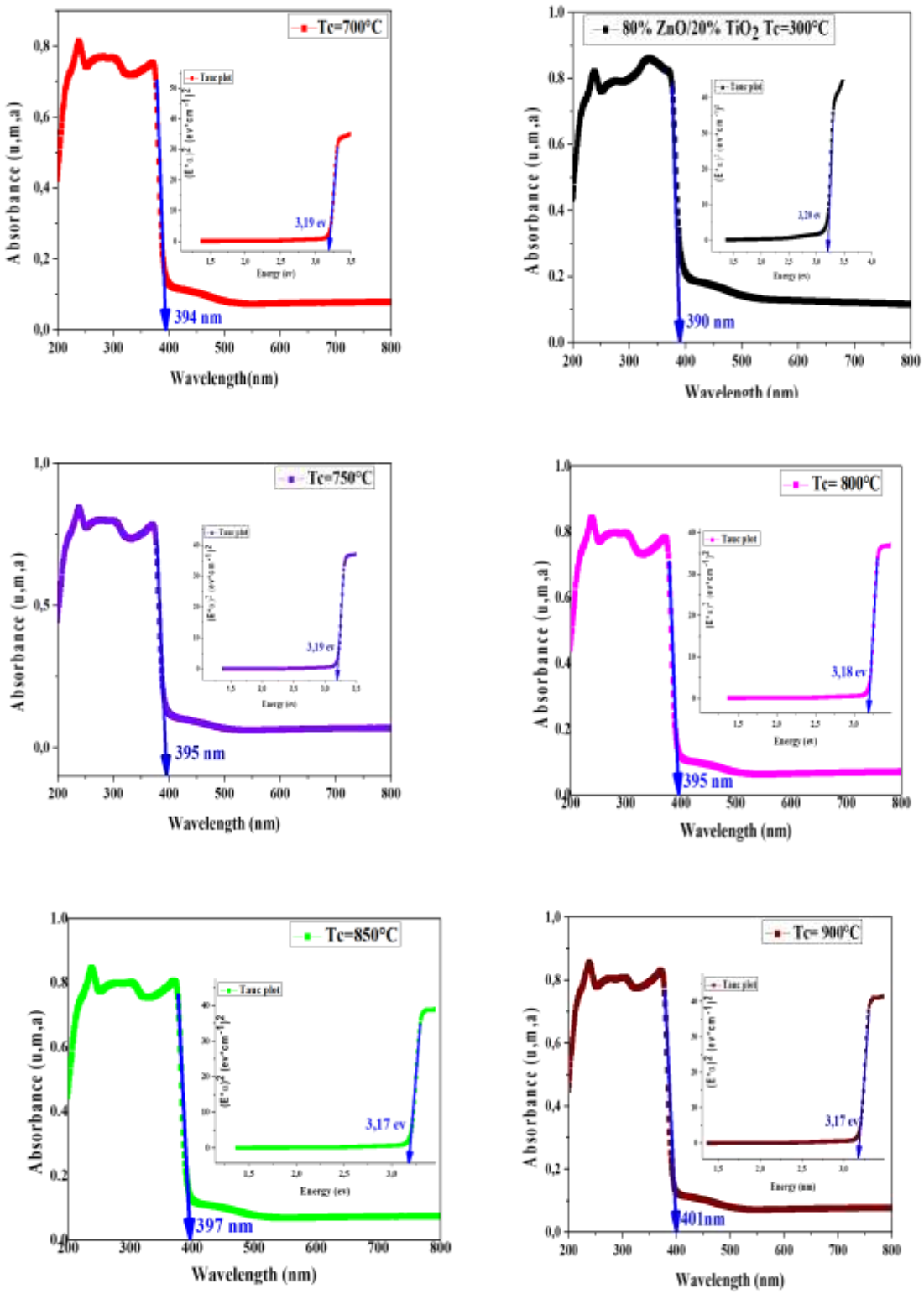


**Figure III.9** Spectral dependence of (αhυ) and photon energy (hυ), used to estimate the band gab value Eg of 80% ZnO/20% $TiO_2$ nanocomposites with different calcination temperatures (700, 750, 800, 850 and 900°C).

### III.1.2.2. Gab energy estimate

The band gab energy Eg was Obtained from the interception of the linear portion of $(\alpha h\upsilon)^2$ as function of $(h\upsilon)$, using Tauc method Eq III.10. The Tauc curves have been shown in **Figure III.10.**

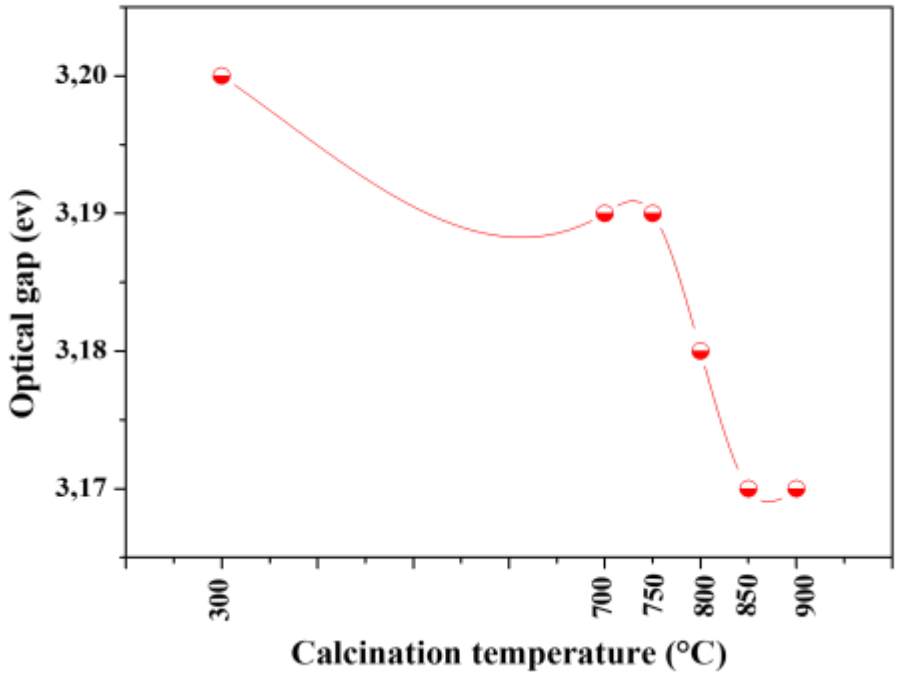


**Figure III.10.** Variation of band gab energy Eg for 80% ZnO/20% $TiO_2$ nanocomposite in different calcination temperatures (300°C, 700, 750, 800, 850 and 900°C)

**Figure III.10** shows the variation of the optical gap of (80% ZnO and 20% $TiO_2$) nanocomposite as function of different calcination temperatures (300, 700, 750, 800, 850 and 900°C, the values of the optical gaps obtained are 3.20, 3.19, 3.19, 3.17 and 3.17 eV respectively, which are consistent with the values found in the literature [6]. We find that the optical gap decreases with the increase in the calcination temperature.

## III.3. Optical properties determined from infrared spectroscopy (FTIR)

**Figure III.11** shows FTIR spectra at the wavenumber 350-4000 $cm^{-1}$ for identified the functional groups and vibrational bonds of nanocomposite ZnO/$TiO_2$.

Fourier transform infrared spectroscopy (FTIR) is an effective tool used to identify functional groups present in the materials under study, identify existing phases and detect impurities. Vibration modes of chemical bonds present in powders prepared were analyzed from the FTIR spectrum.

The absorbance bonds around 464 ,493 and 578 $cm^{-1}$ corresponding to the vibration bond of Zn-O [7].The bond around 1404 $cm^{-1}$corresponding to the vibration of Ti-O[8], and the peak at 736 $cm^{-1}$corresponding to the O-Ti-O band [9],and the bond around 1215$cm^{-1}$ correspond to $Zn_2TiO_4$ phase [10],the little peaks between 1556 and 1735 $cm^{-1}$ corresponding to the vibrations of N-O and C=O. A weak infrared peak at 2350 $cm^{-1}$ probably due to the $CO_2$ vibration bond absorbed during calcination process. The peak at 2931 $cm^{-1}$ is mainly due to the stretching vibration of C-H bond from the absorption of the alkane groups [11].

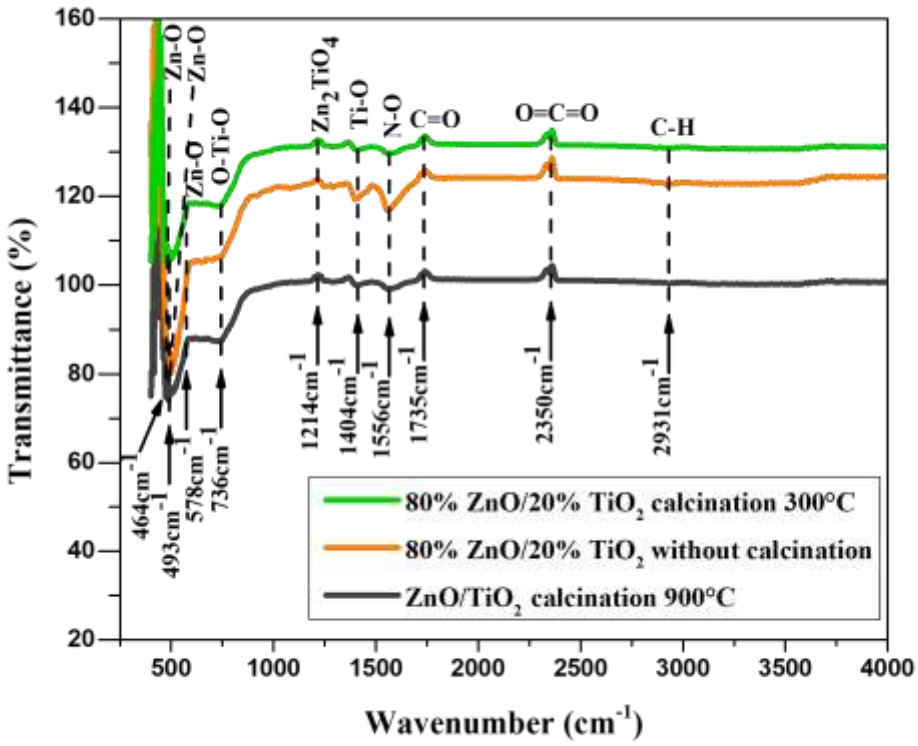


**Figure III.11.** IR spectra of (80%ZnO/20%$TiO_2$) nanocomposite when calcining in 300 and 900 °C, and without calcination.

## III.4. photocatalytic application

**Figure III 12 and 13** show the time course of the photodegradation of methyl orange (MO) with an initial concentration of 17 mg/ml , under UV light for (i) different nanocomposites; 80%ZnO/20%$TiO_2$ ; 65% ZnO/35%$TiO_2$ ; 75%ZnO/35%$TiO_2$ and (ii) different (80%ZnO/20%$TiO_2$) nanocomposite calcined in 300, 700 and 800 °C

We note that after 100 min of UV radiation, the concentration ratio (C/C0) decreases from 1 to 0.2. This indicates that the concentration of methyl orange in the solution decreases, under illumination, during 100 min

It is clear that the nanocomposites (75%ZnO/35%$TiO_2$) and (80%ZnO/20%$TiO_2$) calcined in 850°c give the lowest concentration ratio and therefore the best photocatalytic degradation. This is due to the low optical gap of the samples [(75%ZnO/35%$TiO_2$) and (80%ZnO/20$TiO_2$) calcined in 800°c].

Less is the optical gap, more is the lifetime of photocarriers (less is the recombination rate of photocarriers) and hence the best photodegradation of methyl orange MO

We can explain the process of photocatalytic degradation as follows:

When the (ZnO/$TiO_2$) based nanocomposite absorbs photons with energy hυ>Eg, an electron moves from the BV to the BC, creating an h+ oxidation site and an e- reduction site.

$$NC(h\vartheta) \rightarrow NC + h^+(BV) + e^-(BC) \ldots\ldots\ldots \text{III. 15}$$

The h+ holes react with electron donors such as water, adsorbed $OH^-$ anions and organic products R which are also adsorbed on the surface of the nanocomposite.

These different reactions will then form hydroxyl radicals $OH^{\cdot}$ and $R^{\cdot}$, according to the reactions:

$(H_2O_{ads} + h^+ \rightarrow H^+ + OH^{\cdot}_{ads})$, $(OH^-_{ads} + h^+ \rightarrow OH^{\cdot}_{ads})$ and $(R_{ads} + h^+ \rightarrow R^{\cdot}_{ads})$.

Electrons in BC react with electron acceptors such as oxygen to produce superoxide radicals. The following reaction ($O_2 + e^- \rightarrow O^{\cdot}_2$) is very important because it limits the recombination of charges.

Les $OH^{\bullet}$, $O^{\bullet}_2$, $R^{\bullet}$ are very oxidizing radicals, and can decompose MO. Water and carbon dioxide are the end products.

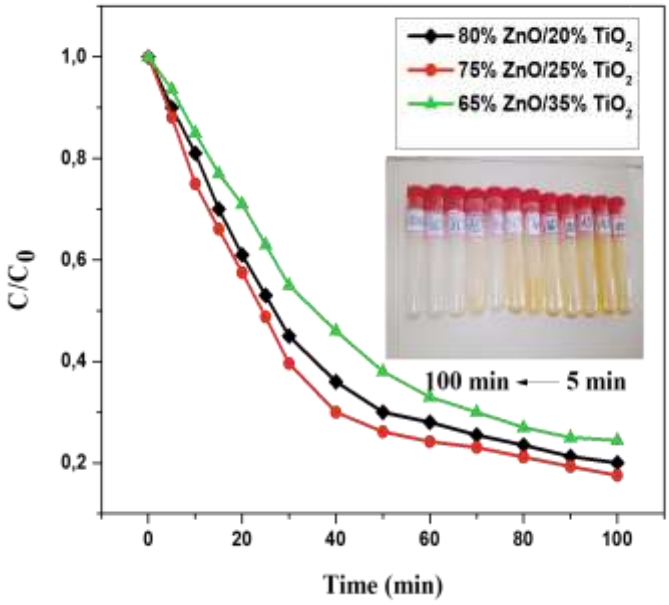


**Figure III.12.** Time course of the photodegradation of methyl orange (MO) with an initial concentration of 17 mg/ml , under UV light for different samples ; 80%ZnO/20%$TiO_2$ ; 65%ZnO/35%$TiO_2$ ; 75%ZnO/25%$TiO_2$

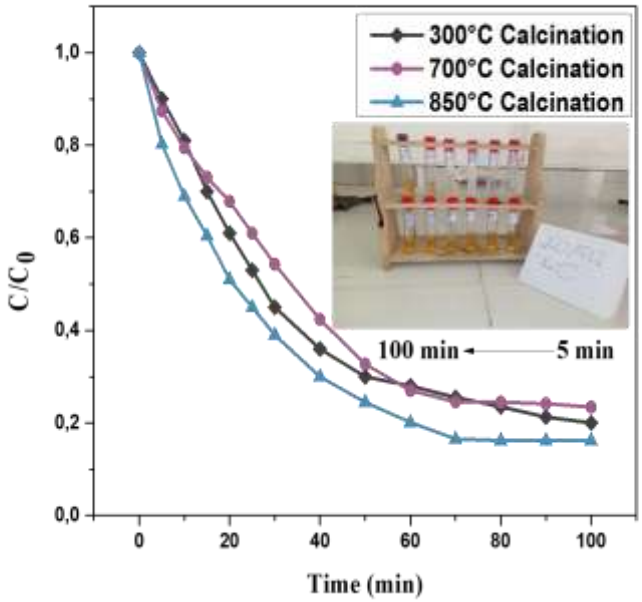


**Figure III.13.** Time course of the photodegradation of methyl orange (MO) with an initial concentration of 17 mg/ml , under UV light for different (80%ZnO/20%$TiO_2$) nanocomposite calcined in 300, 700 and 800 °C.

## III.5. Conclusion

After the preparation and characterization of the two series of prepared sample; (i) 85%ZnO/15%$TiO_2$, 80%ZnO/20%$TiO_2$, 75%ZnO/25%$TiO_2$, 65%ZnO/35%$TiO_2$, (ii) in the second series the sample "80%ZnO/20%$TiO_2$" is calcined in different calcinations temperatures (300, 700, 750, 800, 850 and 900°C). This chapter presents the discussion of the results obtained.

- The XRD spectra of (ZnO/$TiO_2$) nanocomposites exhibit a presence of the two phases which are hexagonal phase of ZnO and cubic phase of $Zn_2TiO_4$.

- Generally (ZnO/$TiO_2$) nanocomposites show (i) a clear absorption edge in the wavelength range of UV [200 nm- 400nm] (ii) significant absorbance around 0.8 in the ultra violet range (200-400nm) .
- In all samples the optical gaps obtained are around 3.21 and 3.17 eV.
- The absorbance bands around 464, 493 and 578 $cm^{-1}$ corresponding to the vibration bond of Zn-O.
- The bands around 1404 $cm^{-1}$corresponding to the vibration of Ti-O and the peak at 736 $cm^{-1}$correspond to the O-Ti-O band.
- The bond around 1214$cm^{-1}$ corresponding to $Zn_2TiO_4$ phase.

- The nanocomposites (75%ZnO/35%$TiO_2$) and (80%ZnO/20$TiO_2$) calcined in 850°c give the lowest concentration ratio and therefore the best photocatalytic degradation. This is due to the low optical gap of the samples [(75%ZnO/35%$TiO_2$) and (80%ZnO/20$TiO_2$) calcined in 850°C].

**References**

[1] https://glossary.periodni.com/glossary.php?en=simple+cubic+lattice.

[2] M.M. Ali, M. Haque, M.H. Kabir, M.A. Kaiyum, M.S. Rahman, Nano synthesis of ZnO–$TiO_2$ composites by sol-gel method and evaluation of their antibacterial, optical and photocatalytic activities, Results in Materials 11(2021)100199.

[3]https://www.researchgate.net/figure/Relationship-between-the-cubic-and-trigonallattice-parameters-of-the-diamond-lattice-V_fig3_244748942

[4] H. Chriet, H. Moualkia, R. Barille, M. Zaabat, O. Mahroua, M. Trari, Morphological, Structural and optical Characterizations of Zn-doped CdS Buffer Layer Elaborated by Chemical Bath Deposition, World Scientific, Review and Letters, 2050009 (10 pages).

[5] N.Hellen, H. Park, K.N. Kim, Characterization of ZnO/$TiO_2$Nanocomposite prepared via the Sol –Gel Method, Journal of the Korean Ceramic Society 55(2018) 140-144.

[6] J.J. Reinosa, P. Leret, C.M. Álvarez-Docio a , A .D.Campo a ,J. F.Fernández, Enhancement of UV absorption behavior inZnO–$TiO_2$ composites, boletín de la sociedadespañola de cerámica y vidrio,55 (2016) 55–62.

[7] A. Gunasekaran , A.K.Rajamani, C. Masilamani,I. Chinnappan, U.Ramamoorthy, K. Kaviyarasu, Synthesis and Characterization of ZnO Doped $TiO_2$Nanocomposites for Their Potential Photocatalytic and Antimicrobial Applications, Catalysts, ( 2023).

[8] A. Leon, P. Reuquen, C. Garin, R. Segura, P. Vargas, P. Zapata, P.A. Orihuela, FTIR and Raman characterization of $TiO_2$ nanoparticles coated with polyethylene glycol as carrier for 2-methoxyestradiol, Applied sciences, 7(1) (2017) 49.

[9] S. Bagheri, K. Shameli, S.B.A. Hamid, Synthesis and characterization of anatase titanium dioxide nanoparticles using egg white solution via sol-gel method, J. Chem. 2013 (2013) 848205. https://doi.org/10.1155/2013/848205.

[10]L. Nikam, R. Panmanda , S. Kadam, S. Naik, B. Kale, Enhanced hydrogen production under visible light source and dye degradation under natural sunlight using nanostructured doped zinc orthotitanates, (2015).

[11] https://www.sigmaaldrich.com/DZ/fr/technical-documents/technical-article/analytical-chemistry/photometry-and-reflectometry/ir-spectrum-

# General Conclusion

This work focuses on the Preparation by Sol- Gel Process of $ZnO/TiO_2$ Nanocomposite and its Activity for Methyl Orange Degradation. This work is carried out in the following laboratories:

- Laboratory of materials and structure of electromechanical systems and their reliability (LMSESR), University of Larbi Ben M'hidi Oum El Bouaghi –Algeria-.
- Applied Chemistry and Materials Technology Laboratory (ACMTL), Larbi Ben M'hidi Oum el Bouaghi University -Algeria-.
- Laboratory of active components and materials Larbi Ben M'hidi Oum el Bouaghi University -Algeria-.
- Chemistry-physics laboratory, University of Hadj Lakhder Batna -1- Algeria.

We prepared two sets (series) of samples; in the first series we varied the composition of ZnO and $TiO_2$ to obtain the nanocomposites of $ZnO/TiO_2$. ZnO percentages are: 85, 80, 75 and 65%, $TiO_2$ percentages are: 15, 20, 25 and 35%. The different samples with the different percentages are: 85%ZnO/15%$TiO_2$, 80%ZnO/20%$TiO_2$, 75%ZnO/25%$TiO_2$, 65%ZnO/35%$TiO_2$, these samples are calcined in low temperature of 300°C, the calcination time is two hours. However, in the second series the sample "80%ZnO/20%$TiO_2$"is calcined in different calcinations temperatures (300, 700, 750, 800, 850 and 900°C), the calcinations time is two hours.

The prepared samples were examined and characterized using X-ray diffraction meter (XRD), UV-VIS spectrometer, Fourier Transform Infrared Spectroscopy FTIR. The prepared samples are used in the potocatalytic degradation of methyl orange under UV irradiation; the most important results obtained can be summarized as follows:

- The XRD spectra of ($ZnO/TiO_2$) nanocomposites exhibit a presence of the two phases which are hexagonal phase of ZnO and cubic phase of $Zn_2TiO_4$.
- The diffraction spectra of the calcined samples in temperatures above 300°C show the emergence of peaks located at 2θ=30.63°, 43.26° and 53.38° corresponding to planes 220),( 400) ,(422) of the $Zn_2TiO_4$ phase.

- The average crystallite size in the hexagonal phase of ZnO and the crystallite size in the $Zn_2TiO_4$ phase are not changed with the percentages of ZnO and $TiO_2$, their values are 22,040 nm and 19.844 nm respectively.

- For Samples calcined in (700-900 nm), the average crystallite size in the ZnO hexagonal phase is equal to 16.69 nm. However, the average crystallite size in the $Zn_2TiO_4$ phase are not changed with the calcinations temperatures, it is equal to 16.04 nm.

- In the sample calcined in 300°C the average crystallite size in the ZnO hexagonal phase and the $Zn_2TiO_4$ phase are equal to 701.25 nm and 22.72 nm, respectively.

- Generally ($ZnO/TiO_2$) nanocomposites show (i) a clear absorption edge in the wavelength range of UV [200 nm- 400 nm] (ii) significant absorbance around 0.8 in the ultra violet range (200-400nm) which allows this nanocomposite to be used in important applications such as protection against solar radiation.
- The values of the optical gaps obtained for (85% ZnO/15% $TiO_2$) ,(80% ZnO/20% $TiO_2$) ,(75% ZnO/25% $TiO_2$) ,(65% ZnO/35% $TiO_2$) are 3.20, 3.21, 3.19 and 3.20 respectively
- The values of the optical gaps obtained for (80% ZnO and 20% $TiO_2$) nanocomposite calcined in (300, 700, 750, 800, 850 and 900°C are 3.20, 3.19, 3.19, 3.17 and 3.17 ev respectively.
- The optical gap decreases with the increase in the calcination temperature.
- Optical properties determined from infrared spectroscopy (FTIR).
- The absorbance bands around 464, 493 and 578 $cm^{-1}$ corresponding to the vibration bond of Zn-O.
- The band around 1404 $cm^{-1}$corresponding to the vibration of Ti-O and the peak at 736 $cm^{-1}$correspond to the O-Ti-O band.
- The band around 1214$cm^{-1}$ corresponding to $Zn_2TiO_4$ phase.
- The little peaks between 1556 and 1735 $cm^{-1}$ corresponding to the vibrations of N-O and C=O.
- A weak infrared peak at 2350 $cm^{-1}$ probably due to the $CO_2$ vibration bond absorbed during calcination process.

- Nanocomposites prepared with (i) different percentages; 80%ZnO/20%$TiO_2$; 65%ZnO/35%$TiO_2$; 75% ZnO/25%$TiO_2$ and (ii) different (80%ZnO/20%$TiO_2$) nanocomposite calcined in 300, 700 and 800 °C, are used for the photodegradation of methyl orange (MO) under UV light, after 100 min of UV radiation, the concentration

ratio (C/C0) decreases from 1 to 0.2, which indicates that the concentration of methyl orange in the solution decreases.

- The nanocomposites (75%ZnO/35%$TiO_2$) and (80%ZnO/20%$TiO_2$) calcined in 850°c give the lowest concentration ratio and therefore the best photocatalytic degradation. This is due to the low optical gap of the samples [(75%ZnO/35%$TiO_2$) and (80%ZnO/20%$TiO_2$) calcined in 850°C].
- Less is the optical gap, more is the lifetime of photocarriers (less is the recombination rate of photocarriers) and hence is the best photodegradation of methyl orange.

## Abstract

This work focuses on the sol-gel preparation of nanocomposites based on ZnO and $TiO_2$. We prepared two sets of samples. For the first, we modified the percentages of ZnO and $TiO_2$, the prepared nanocomposites are (65% ZnO/35% $TiO_2$, 75% ZnO/25% $TiO_2$, 80% ZnO/20% $TiO_2$, 85% ZnO/15% $TiO_2$). While for the second series we varied the calcination temperature from 300°C to 900°C of the nanocomposites (80% ZnO/20% $TiO_2$). The structural and optical properties obtained from the nanocomposites were studied, using respectively the XRD spectrum, and UV-Vis, FTIR. The XRD results give us two phases ZnO and $Zn_2TiO_4$. The UV-visible spectra show that the absorption capacity of the nanocomposites is significantly improved in the visible. The absorption bands for ZnO and $Zn_2TiO_4$ were detected by FTIR analysis. As an application we used ($ZnO$/$TiO_2$) nanocomposites in the photocatalytic degradation of methyl orange. The prepared nanocomposites showed high photocatalytic activity and gave MO dye degradation within 100 min.

**Keywords:** nanocomposites, $ZnO$-$TiO_2$, Sol- gel, photocatalytic heterogeneous, methyl orange

## Résumé

Ce travail porte sur la préparation par sol-gel des nanocomposites à base de ZnO et $TiO_2$. Nous avons préparé deux séries d'échantillons. Pour la première, nous avons modifié les pourcentages du ZnO et du$TiO_2$, les nanocomposites préparés sont (65% ZnO/35% $TiO_2$ ,75% ZnO/25% $TiO_2$ ,80% ZnO/20% $TiO_2$ ,85% ZnO/15% $TiO_2$). Tandis que pour la deuxième série nous avons varié la température de calcination de 300°C à 900°C du nanocomposites (80% ZnO/20% $TiO_2$). Les propriétés structurales, et optiques obtenues des nanocomposites ont été étudiées, en utilisant respectivement le spectre DRX, et UV-Vis, FTIR. Les résultats DRX nous donnent deux phases ZnO et $Zn_2TiO_4$. Les spectres UV-visible montrent que la capacité d'absorption des nanocomposites est significativement améliorée dans le visible. Les bandes d'absorption pour ZnO et $Zn_2TiO_4$ ont été détectés par analyse FTIR. Comme application nous avons utilisé les nanocomposites de ($ZnO$/$TiO_2$) dans la dégradation photocatalytique du méthyle orange. Les nanocomposites préparés ont montré une activité photocatalytique élevée et ont donnéla dégradation du colorant MO en 100 min.

**Mots clés :** nanocomposites, $ZnO$-$TiO_2$, Sol-gel, photocatalytique hétérogène, Méthyle Orange.

**الملخص**

يركز هذا العمل على تحضير لمركبات النانوية على أساس ZnO و$TiO_2$بطريقة سول- جل. قمنا بإعداد مجموعتين من العينات. أولاً ، قمنا بتعديل النسب المئوية من ZnO و $TiO_2$ ، والمركبات النانوية المحضرة هي$85\%ZnO/15\%TiO_2$, $80\%ZnO/20\%TiO_2$, $75\%ZnO/25\%TiO_2$, ($65\%ZnO/35\%TiO_2$,) . بينما بالنسبة للسلسلة الثانية قمنا بتغيير درجة حرارة التكليس من 300 درجة مئوية إلى 900 درجة مئوية للمركبات النانوية ($80\%ZnO/20\%TiO_2$). تمت دراسة الخواص التركيبية والبصرية من المركبات النانوية باستخدام طيف XRD و UV-Vis و FTIR على التوالي. تعطينا نتائج XRD مرحلتين ZnO و $Zn_2TiO_4$. تظهر الأطياف المرئية للأشعة فوق البنفسجية أن قدرة امتصاص المركبات النانوية قد تحسنت بشكل كبير في المرئي. تم الكشف عن نطاقات امتصاص ZnO و $Zn_2TiO_4$ عن طريق تحليل FTIR. كتطبيق استخدمنا مركبات نانوية ($ZnO$ / $TiO_2$) في التحلل التحفيزي لبرتقال الميثيل. أظهرت المركبات النانوية المحضرة نشاط تحفيزي ضوئي عالي وأعطت تحلل صبغة MO في غضون 100 دقيقة.

**الكلمات المفتاحية** : المواد المركبة, $ZnO$-$TiO_2$ , سول-جال, التحفيز الضوئي غير متجانس, برتقالي الميثيل.